

# Sparse Approximate Inference for Spatio-Temporal Point Process Models

Botond Cseke<sup>\*1</sup>, Andrew Zammit-Mangion<sup>†2</sup>, Tom Heskes<sup>‡3</sup>, and Guido Sanguinetti<sup>§1</sup>

<sup>1</sup>School of Informatics, University of Edinburgh

<sup>2</sup>School of Geographical Sciences, University of Bristol

<sup>3</sup>Faculty of Science, Radboud University Nijmegen

May 17, 2022

---

<sup>\*</sup>Email: bcseke@inf.ed.ac.uk. B. Cs. is funded by BBSRC under grant BB/I004777/1.

<sup>†</sup>Email: a.zammitmangion@bristol.ac.uk. A. Z.-M. is funded by NERC under grant NE/I027401/1.

<sup>‡</sup>Email: t.heskes@science.ru.nl. T.H. is professor in Artificial Intelligence at R.U.N.

<sup>§</sup>Email: gsanguin@inf.ed.ac.uk. G.S. is funded by ERC under grant MLCS-306999.

## Abstract

Spatio-temporal point process models play a central role in the analysis of spatially distributed systems in several disciplines. Yet, inference remains computationally challenging both due to the high resolution modelling generally required by large data sets and the analytically intractable likelihood function. Here, we exploit the sparsity structure typical of (spatially) discretised log-Gaussian Cox process models by using expectation constrained approximate inference. The resulting family of approximate message passing algorithms scale well with the state dimension and the length of the temporal horizon with moderate loss in distributional accuracy. They hence provide a flexible and faster alternative to both non-linear filtering-smoothing type algorithms and to approaches that implement the Laplace method or expectation propagation on (block) sparse latent Gaussian models. We infer the parameters of the latent Gaussian model by a structured variational Bayes approach embedded into the expectation constrained inference framework. We demonstrate the proposed method on simulation studies with both Gaussian and point-process observations and apply it to the reconstruction of conflict intensity levels in Afghanistan from a WikiLeaks data set.

*Keywords:* latent Gaussian models, log-Gaussian Cox process, variational approximate inference, expectation propagation, sparse approximate inference, structure learning, conflict analysis.

# 1 Introduction

Dynamic models of spatially distributed systems and point processes are omnipresent in scientific applications of computational statistics, ranging from environmental sciences (Wikle et al., 2001) to epidemiology (Diggle et al., 2005) and ecology (Hooten and Wikle, 2008) to name but a few. The prevalence of such data is dramatically increasing due to advances in remote sensing technologies, and novel application domains are fast emerging in the social sciences due to the large scale data sets collected e.g. through social networks. Despite their importance, inference in these systems remains computationally challenging. Markov chain Monte Carlo (MCMC) is frequently employed and has desirable asymptotic properties; however, despite considerable advances (Andrieu et al., 2010; Girolami and Calderhead, 2011), the computational costs of sampling approaches remain problematically high for high dimensional heterogeneous data sets. Consequently, deterministic approximate inference methods are rapidly gaining popularity in this field. These approaches can be classified as dynamic or static: the former class consists of filtering-smoothing type approaches such as the variational approach in Zammit-Mangion et al. (2012a), the expectation propagation (EP) algorithm (e.g. Ypma and Heskes, 2005) or EP exploiting low rank approximations (Hartikainen et al., 2011). The static approaches cast the (time discretised) model as a latent (sparse) Gaussian block model and apply the Laplace method (Rue et al., 2009; Lindgren et al., 2011) or a corresponding EP algorithm (e.g. Cseke and Heskes, 2011). The computational cost of inference in static models is dominated by a sparse partial matrix inversion using sparse Cholesky factorisation (Takahashi et al., 1973); these costs may become untenable for very high dimensions, and it is not always clear how further (robust) approximations could be made to ameliorate these problems (e.g. Wist and Rue, 2006; Simpson et al., 2013).

In this paper we derive a joint inference method for both state space and parameter inference. For state space inference we propose an approximate message passing algorithm that combines the typical advantages of message passing algorithms (filtering-smoothing in the temporal case) like scalability w.r.t. the time horizon, flexibility w.r.t. message scheduling, and that also exploits the sparsity (in canonical/precision parameters) of the underlying latent Gaussian model. The approach we take exploits sparsity by using sparse Cholesky factorisations and sparse partial matrix inversions as in Rue et al. (2009); Simpson et al. (2012) and Cseke and Heskes (2011), however, the significant difference is that they are performed not on the block model, but on the matrices resulting from the (approximate) marginals computed during message passing. Ideally, one would like to use a variant of non-linear filtering-smoothing, however, these algorithms typically operate on moment parameters and/or involve operations that tend to destroy sparsity such as matrix multiplication and marginalisation of Gaussians. We avoid these operations by formulating the problem in the expectation constrained approximate inference framework (Heskes et al., 2005; Opper and Winther, 2005). This framework recasts the inference or marginalisation problem as an optimisation over approximate marginals that are constrained to satisfy weak consistency constraints (expectation constraints). The objective is derived from the variational framework and resembles the variational free energies used in statistical physics (e.g. Yedidia et al., 2000). This formulation allows us to deal with non-Gaussianity and also enables us to control the accuracy and computational complexity through the choice of the expectation constraints. As a result, we propose a message passing algorithm that does not explicitly

perform marginalisation—it is replaced by sparse partial inversion—and operates through forward and backward messages that have sparse precision structures. The complexity of the local computations then depends on the graph structure of the expectation constraints we impose on the approximate two time-slice marginals. The method naturally allows for a compromise between computation speed and accuracy. To show this we introduce a class of constraints that result in Gaussian messages having precision structures which are increasingly representative: (i) diagonal (factored messages), (ii) spanning tree (iii) chordal and finally (iv) fully connected (full messages). The latter corresponds to the filtering-smoothing type algorithm that is using expectation propagation for the non-Gaussian parts. An algorithmically similar approach to (i) for discrete dynamic Bayesian networks was proposed in [Murphy and Weiss \(2001\)](#). Comparisons in simulated case studies show that the proposed algorithms scale well and, depending on the complexity of the messages, we can carry out approximate inference on hundreds or a few thousands of state variables and hundreds of time-steps with reasonable time and memory requirements. To learn the model parameters of the latent Gaussian field, we use a structured variational Bayes approach that can be naturally embedded in the expectation constrained approximate inference framework.

The text is structured as follows. In [Section 2](#) we introduce log-Gaussian Cox processes and present the discretisation and approximation steps that simplify this model to a dynamic latent Gaussian model with non-Gaussian pseudo-observation terms. In [Section 3](#) we derive a class of dynamic message passing algorithms that exploit the sparsity resulting from the discretisation. In [Section 4](#) we discuss the performance of these algorithms and apply them to the WikiLeaks Afghan War Diary, a data set containing tens of thousands of events from the Afghan war. Due to the high resolution provided by the model, we can capture micro-dynamic effects and show that these identify sources and targets of conflict diffusion.

## 2 Model

In this paper we are interested in the dynamic modelling of two dimensional point patterns. The data consists of location and time stamped events  $\mathcal{Y} = \{(\mathbf{s}_i, t_i)\}_i$  where the locations  $\mathbf{s}_i$  are points in a two dimensional domain  $\mathbf{s}_i \in \mathcal{S}$  and the time-stamps  $t_i$  are in a time interval  $\mathcal{T} = [0, \max_i(t_i)]$ . In order to model this type of data, we use both spatially and temporally discretised log-Gaussian Cox process models ([Møller et al., 1998](#); [Brix and Møller, 2001](#)). We discretise the domain  $\mathcal{S}$  by using a triangular grid and define the corresponding piecewise linear finite element basis  $\{\phi_i(\mathbf{s})\}_i$ . We discretise time by dividing the time interval  $\mathcal{T}$  into  $T$  equal time windows  $[t\Delta_t, (t+1)\Delta_t]$  with  $T\Delta_t = \max_i(t_i)$ . We then consider that the time-stamps within each window are equal, that is  $t_i = t_j$  for all  $t_i, t_j \in [t\Delta_t, (t+1)\Delta_t]$ . As a result, we redefine our dataset as  $\mathcal{Y} = \cup_t \mathcal{Y}_t$  where each  $\mathcal{Y}_t$  denotes the events in time interval  $[t\Delta_t, (t+1)\Delta_t]$ , all having the same time-stamp  $t\Delta_t$ . The choice of  $\Delta_t$  is often determined by the application and although it can be critical from the computational point of view, it is beyond the scope of this paper to address this problem.

We define the log intensity function of the point process as a linear combination of the basis functions  $\phi_i$ , that is  $\lambda(\mathbf{s}, t) = \exp\{\mathbf{x}_t^T \boldsymbol{\phi}(\mathbf{s})\}$  and assume that the weights  $\mathbf{x}_t$  follow a linear dynamical system

$$\mathbf{x}_{t+1} = \mathbf{A}\mathbf{x}_t + \boldsymbol{\epsilon}_t, \quad (1)$$



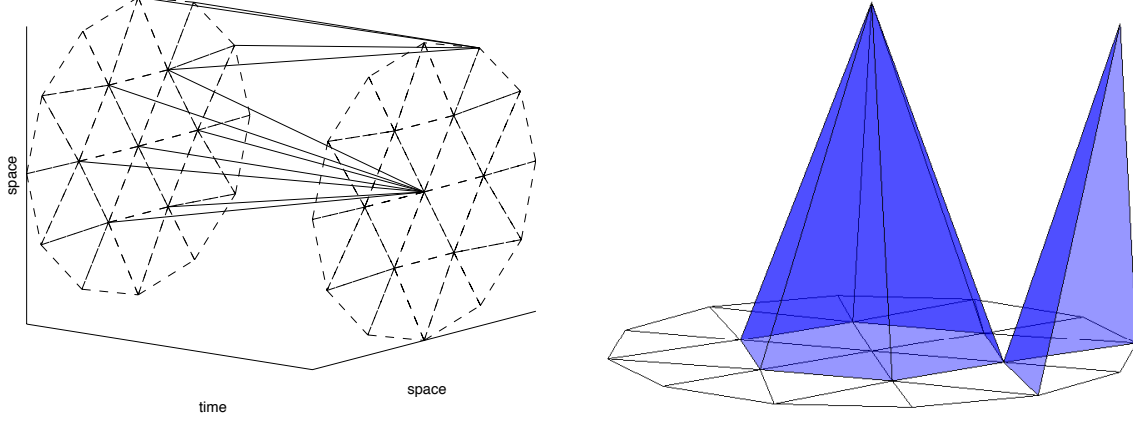


Figure 1: An illustration of the spatio-temporal discretisation. The right panel illustrates two basis functions defined according to the triangular finite element spatial discretisation. The bases are shown for two nodes/vertices, one in the interior and one on the boundary of the domain. The left panel illustrates the temporal connectivity for some of the nodes resulting from the spatio-temporal discretisation described in Section 2. Similarly, the temporal connectivities are shown only for an interior and a boundary node/vertex.

where  $\epsilon_t \sim \mathcal{N}(\mathbf{0}, \mathbf{Q}^{-1})$  with both  $\mathbf{A}$  and  $\mathbf{Q}$  sparse. These types of models for the log intensity  $u(\mathbf{s}, t) = \log \lambda(\mathbf{s}, t)$  can be obtained from spatio-temporal models commonly employed in practice, such as the integro-difference equation (IDE) (Wikle, 2002), and the stochastic partial differential equation (SPDE) (Zammit-Mangion et al., 2012b). Sparsity in  $\mathbf{A}$  and  $\mathbf{Q}$  follows either from gridding the domain or from employing a Galerkin reduction on an infinite-dimensional system in  $u(\mathbf{s}, t)$ ,  $\mathbf{s} \in \mathcal{S}, t \in \mathcal{T}$  using the basis functions  $\{\phi_i(\mathbf{s})\}_i$ . In both cases we can write the approximate field as  $u(\mathbf{s}, t) \approx \mathbf{x}_t^T \boldsymbol{\phi}(\mathbf{s})$ . Note that this field is continuous but not differentiable (see the illustration in Figure 1). Stronger smoothness properties can be achieved by convolving the linear basis to obtain spline basis sets. This, however, also leads to less sparsity in  $\mathbf{A}$  and  $\mathbf{Q}$ .

The likelihood function for a general intensity  $\lambda(\mathbf{s}, t)$  can be written as

$$p(\mathcal{Y}|\lambda) \propto \exp \left\{ - \int_{\mathcal{S} \times \mathcal{T}} ds dt \lambda(\mathbf{s}, t) \right\} \times \prod_i \lambda(\mathbf{s}_i, t_i).$$

By using our assumptions about the spatial and temporal discretisation, we approximate this likelihood by writing  $p(\mathcal{Y}|\lambda) \propto \prod_t p(\mathcal{Y}_t|\mathbf{x}_t)$  where

$$\begin{aligned} p(\mathcal{Y}_t|\mathbf{x}_t) &\propto \exp \left\{ - \Delta_t \int_{\mathcal{S}} d\mathbf{s} e^{\mathbf{x}_t^T \boldsymbol{\phi}(\mathbf{s})} \right\} \times \prod_{(\mathbf{s}_i, t_i) \in \mathcal{Y}_t} e^{\mathbf{x}_t^T \boldsymbol{\phi}(\mathbf{s}_i)} \\ &= L_1(\mathbf{x}_t) \times L_2(\mathbf{x}_t; \mathcal{Y}_t). \end{aligned} \quad (2)$$

This likelihood can be split into two components: the first component  $L_1(\mathbf{x}_t)$  is directly related to the *void probability* of the process. We adopt the approach in Simpson et al.

(2011) and approximate the integral as:

$$\begin{aligned}\log L_1(\mathbf{x}_t) &\approx -\Delta_t \sum_{i=1}^p \tilde{\eta}_i \exp(\boldsymbol{\phi}^T(\bar{\mathbf{s}}_i) \mathbf{x}_t) \\ &= -\boldsymbol{\eta}^T \exp(\mathbf{C}_1 \mathbf{x}_t),\end{aligned}\tag{3}$$

where the vector  $\boldsymbol{\eta}$  denotes the integration weights  $\Delta_t \tilde{\boldsymbol{\eta}}$  and the matrix  $\mathbf{C}_1 = [\boldsymbol{\phi}(\bar{\mathbf{s}}_1) \dots \boldsymbol{\phi}(\bar{\mathbf{s}}_p)]^T$  contains the values of the basis at the chosen  $p$  integration points  $\{\bar{\mathbf{s}}_i\}_{i=1}^p$ . The second component of the likelihood,  $L_2(\mathbf{x}_t; \mathcal{Y}_t)$ , denotes the contributions from the observed events and can be represented as

$$\log L_2(\mathbf{x}_t; \mathcal{Y}_t) = \sum_{j \in I_t} \boldsymbol{\phi}^T(\mathbf{s}_j) \mathbf{x}_t = \mathbf{1}^T \mathbf{C}_2(\mathcal{Y}_t) \mathbf{x}_t,\tag{4}$$

where  $\mathbf{C}_2(\mathcal{Y}_t)^T = [\boldsymbol{\phi}(\mathbf{s}_i)]_{i \in I_t}$ . The approximate log-likelihood can hence be written, up to a proportionality constant, as

$$\log p(\mathcal{Y}_t | \mathbf{x}_t) \approx -\boldsymbol{\eta}^T \exp(\mathbf{C}_1 \mathbf{x}_t) + \mathbf{1}^T \mathbf{C}_2(\mathcal{Y}_t) \mathbf{x}_t.\tag{5}$$

Both compact basis functions and gridded domains induce sparsity into the observation matrices  $\mathbf{C}_1$  and  $\mathbf{C}_2$ . In particular, if one chooses the integration points to be the vertices of a triangulation or the centres of gridded cells, then  $\mathbf{C}_1$  simplifies to the identity matrix  $\mathbf{I}_{n \times n}$  where  $n = p$ . The integration weights  $\boldsymbol{\eta}$  then correspond to the time-lag scaled volumes of the basis with unit weight. In addition,  $\mathbf{C}_2(\mathcal{Y}_t)$  is again sparse with at most one non-zero element in each row for the gridded case and three non-zero elements per row for the triangulated case. As a consequence, the spatial discretisation results in a latent Gaussian model. By using the above cited approach to the approximation of the integral, we arrive at a diagonal  $\mathbf{C}_1$ . This, together with the linear nature of (4), shows that the non-Gaussian terms depend only on  $x_t^j$ . In the following we use  $\psi_{t,j}(x_t^j) = \exp\{-\eta_j \exp(x_t^j)\}$  and introduce  $\mathbf{X} = \{\mathbf{x}_t\}_{t=1}^T$ ,  $\mathcal{Y} = \{\mathcal{Y}_t\}_{t=1}^T$  and  $\mathbf{h}_t = \mathbf{1}^T \mathbf{C}_2(\mathcal{Y}_t)$  to ease the exposition.

In our setting  $\mathbf{Q}$  is a sparse, typically diagonal matrix, while the structure of the transition matrix  $\mathbf{A}$  follows the structure of the neighbourhood graph that results from the discretisation. In most practical cases  $\mathbf{A}$  has a relatively small number of structurally non-zero elements (neighbourhood structure) most of which are also very small or zero. For this reason we impose a spike and slab prior on its structurally non-zero elements. We do this by introducing a set of binary auxiliary variables  $Z = \{z_{ij}\}_{i,j}$  with  $z_{ij} \in \{0, 1\}$  and  $j \in I_i$ , where  $I_i = \text{supp}(\mathbf{a}_{i,\cdot})$  is the index set of the structurally non-zero elements in the  $i^{\text{th}}$  row  $\mathbf{a}_{i,\cdot}$  of  $\mathbf{A}$ . We then define the conditional prior  $p_0(a_{ij} | z_{ij}, v_{\text{slab}}) = N(a_{ij}; 0, z_{ij} v_{\text{slab}})$  and assume a Bernoulli prior  $p_0(z_{ij} | p_{\text{slab}}) = \text{Ber}(z_{ij}; p_{\text{slab}})$ . Consequently, we can use the posterior distribution of the variable  $z_{ij}$  to quantify the relevance of the transition coefficient  $a_{ij}$ . By choosing  $p_{\text{slab}} = 1$  we can revert to the default case of conjugate Gaussian priors. We use a Gamma prior  $\text{Gam}(q_{ii}; k, \tau)$  for the diagonal elements of the precision matrix  $\mathbf{Q}$ .

With the above assumptions we can formulate the joint probabilistic model

$$\begin{aligned}p(\mathcal{Y}, \mathbf{X}, \mathbf{A}, \mathbf{Z}, \mathbf{Q} | \boldsymbol{\theta}) &= p_0(\mathbf{x}_1) \prod_t p(\mathbf{x}_{t+1} | \mathbf{x}_t, \mathbf{A}, \mathbf{Q}) \prod_j \tilde{\psi}_{t+1,j}(x_{t+1}^j) \\ &\times \prod_{i \sim j} p_0(a_{ij} | z_{ij}, \boldsymbol{\theta}) p_0(z_{ij} | \boldsymbol{\theta}) \prod_i p_0(q_{i,i} | \boldsymbol{\theta})\end{aligned}\tag{6}$$

with  $\boldsymbol{\theta} = \{\mathbf{m}_1, \mathbf{V}_1, \boldsymbol{\eta}, v_{\text{slab}}, p_{\text{slab}}, k, \tau\}$  collecting the parameters of

$$\begin{aligned}\tilde{\psi}_{t+1,j}(x_{t+1}^j) &\propto e^{h_j x_{t+1}^j - e^{\eta_j x_{t+1}^j}}, \\ &\propto e^{h_j x_{t+1}^j} \psi_{t+1,j}(x_{t+1}^j) \\ p_0(\mathbf{x}_1) &= N(\mathbf{x}_1; \mathbf{m}_1, \mathbf{V}_1), \\ p(\mathbf{x}_{t+1} | \mathbf{x}_t, \mathbf{A}, \mathbf{Q}) &= N(\mathbf{x}_{t+1}; \mathbf{A} \mathbf{x}_t, \mathbf{Q}^{-1}), \\ p_0(a_{ij} | z_{ij}, \boldsymbol{\theta}) &= N(a_{ij}; 0, z_{ij} v_{\text{slab}}), \\ p_0(z_{ij} | \boldsymbol{\theta}) &= \text{Ber}(z_{ij}; p_{\text{slab}}), \\ p_0(q_{ii} | \boldsymbol{\theta}) &= \text{Gam}(q_{ii}; k, \tau).\end{aligned}$$

### 3 Inference

As mentioned in Section 1, the dimension of the state space can be hundreds or thousands. In such models sampling from the posterior can be computationally demanding. For this reason, we resort to variational approximate inference methods and we seek structured factorised approximations to the posterior distribution. Variational approximate inference methods formulate inference as an optimisation problem by using the Kullback-Leibler divergence  $D[\cdot || p]$  as optimisation objective. These methods have been successfully applied in many areas of engineering and machine learning where large scale probabilistic models are common. To approximate the posterior distribution  $p(\mathbf{X}, \mathbf{A}, \mathbf{Z}, \mathbf{Q} | \mathcal{Y}, \boldsymbol{\theta})$ <sup>1</sup> in (25) we seek an approximation where we postulate the factorisation  $q(\mathbf{X}, \mathbf{A}, \mathbf{Z}, \mathbf{Q} | \boldsymbol{\theta}) = q_X(\mathbf{X} | \boldsymbol{\theta}) q_{AZ}(\mathbf{A}, \mathbf{Z} | \boldsymbol{\theta}) q_Q(\mathbf{Q} | \boldsymbol{\theta})$  and minimise  $D[q_X q_{AZ} q_Q || p]$  w.r.t.  $q_X, q_{AZ}$  and  $q_Q$ . Further factorisations follow from the independence relations in the posterior distribution.

We start from the free form variational updates and introduce the necessary approximation schemes where the computations become intractable. The variational approach can be formally written as

$$\underset{q_X, q_{AZ}, q_Q}{\text{minimise}} D[q_X(\mathbf{X}) q_{AZ}(\mathbf{A}, \mathbf{Z}) q_Q(\mathbf{Q}) || p(\mathbf{X}, \mathbf{A}, \mathbf{Z}, \mathbf{Q} | \mathcal{Y})]. \quad (7)$$

The optimality conditions result in a component-wise fixed point iteration that is known to correspond to a coordinate descent on the objective in (7). In the case of our model, these optimality conditions read as

$$q_X(\mathbf{X}) \propto p_1(\mathbf{x}_1) \prod_{t,j} \psi_{t+1,j}(x_{t+1}^j) \exp \left\{ \sum_t \langle \log p(\mathbf{x}_{t+1} | \mathbf{x}_t, \mathbf{A}, \mathbf{Q}) \rangle_{q_{AZ}, q_Q} \right\}, \quad (8)$$

$$q_{AZ}(\mathbf{A}, \mathbf{Z}) \propto \prod_{i \sim j} p_0(a_{ij} | z_{ij}) p_0(z_{ij}) \exp \left\{ \sum_t \langle \log p(\mathbf{x}_{t+1} | \mathbf{x}_t, \mathbf{A}, \mathbf{Q}) \rangle_{q_X, q_Q} \right\}, \quad (9)$$

$$q_Q(\mathbf{Q}) \propto \prod_i p_0(q_{ii} | \boldsymbol{\theta}) \exp \left\{ \sum_t \langle \log p(\mathbf{x}_{t+1} | \mathbf{x}_t, \mathbf{A}, \mathbf{Q}) \rangle_{q_X, q_{AZ}} \right\}. \quad (10)$$

Clearly, none of the above densities have a form that would make the required expectation values computationally tractable and thus allowing us to run the variational fixed point

---

<sup>1</sup>In the following we consider  $\boldsymbol{\theta}$  constant and omit it when not necessary.

iteration. For this reason, we propose to compute the required expectations, which are first and second order marginal moments, by applying further approximate inference techniques in the models defined by  $q_X, q_{AZ}$  and  $q_Q$ . To do this we view them from a graphical model (Lauritzen, 1996) or factor graph (Kschischang et al., 2001) perspective and use efficient approximate inference techniques. The approximations we arrive at can be embedded into the wider, principled framework of structured variational approximate inference by using expectation constraints as in Heskes et al. (2005) and Oppor and Winther (2005). In the following sections we present the algorithmic approach. A detailed derivation of the proposed method is given in the Supplementary Material.

### 3.1 The model $q_X$

The model for  $q_X$  is a dynamic latent Gaussian model where the non-Gaussian terms  $\psi_{t,j}(x_t^j)$  depend on only one state space component  $x_t^j$ . The model is tree structured, that is, we have a Gaussian chain structure due to  $\exp\langle\log p(\mathbf{x}_{t+1}|\mathbf{x}_t, \cdot)\rangle_{q_{AZ}, q_Q}$  and non-Gaussian leaves due to  $\tilde{\psi}(x_t^i)$ . In tree structured graphical models inference can be done by using the message passing algorithm (e.g. Lauritzen, 1996) which is a dynamic programming method for summing/integrating out variables to compute the marginal distributions—a classical example being the forward-backward algorithm in dynamic models (chain structured tree graphs). In our model however, the messages can become computationally intractable and one has to resort to approximations. In the following we present the message passing algorithm for  $q_X$  and the approximations we use to compute its marginal densities and moments.

In order to make the message passing tractable we use Gaussian messages between the Gaussian and non-Gaussian terms. Moreover, we propose to use messages with restricted precision structures between the Gaussian factors to exploit sparsity and significantly reduce computing time; the technicalities are presented in Section 3.1.2.

Let us recall that  $\psi_{t+1,j}(x_{t+1}^j) \propto \exp\{-\exp(\eta_j \mathbf{x}_{t+1}^j)\}$  and define the Gaussian terms  $\Psi_{t,t+1}(\mathbf{x}_t, \mathbf{x}_{t+1}) \propto \exp\{\langle\log p(\mathbf{x}_{t+1}|\mathbf{x}_t, \mathbf{A}, \mathbf{Q})\rangle_{q_{AZ}, q_Q}\} \times \exp(\mathbf{x}_{t+1} \cdot \mathbf{h}_{t+1}^y)$  with the additional  $\mathbf{x}_1$  related Gaussian terms attached to  $\Psi_{1,2}(\mathbf{x}_1, \mathbf{x}_2)$ . By using this notation,  $q_X$  reads as

$$q_X(\mathbf{X}) \propto \prod_t \Psi_{t,t+1}(\mathbf{x}_t, \mathbf{x}_{t+1}) \times \prod_{t,j} \psi_{t+1,j}(x_{t+1}^j). \quad (11)$$

The generic message passing algorithm for this tree structured model can be written as

$$\lambda_{t+1,j}^0(x_{t+1}^j) \propto \psi_{t+1,j}(x_{t+1}^j), \quad (12)$$

$$\alpha_{t+1}(\mathbf{x}_{t+1}) \propto \int d\mathbf{x}_t \Psi_{t,t+1}(\mathbf{x}_t, \mathbf{x}_{t+1}) \alpha_t(\mathbf{x}_t) \prod_j \lambda_{t+1,j}^0(x_{t+1}^j), \quad (13)$$

$$\beta_t(\mathbf{x}_t) \propto \int d\mathbf{x}_{t+1} \Psi_{t,t+1}(\mathbf{x}_t, \mathbf{x}_{t+1}) \beta_{t+1}(\mathbf{x}_{t+1}) \prod_j \lambda_{t+1,j}^0(x_{t+1}^j), \quad (14)$$

$$\lambda_{t+1,j}^l(x_{t+1}^j) \propto \int d\mathbf{x}_t d\mathbf{x}_{t+1}^{\setminus j} \Psi_{t,t+1}(\mathbf{x}_t, \mathbf{x}_{t+1}) \alpha_t(\mathbf{x}_t) \beta_{t+1}(\mathbf{x}_{t+1}) \prod_{k \neq j} \lambda_{t+1,k}^0(x_{t+1}^k)$$

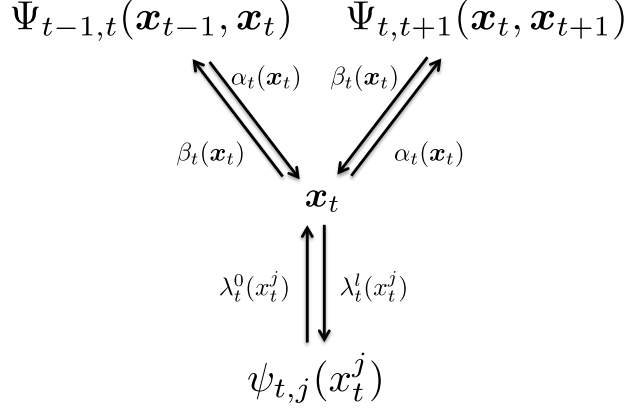


Figure 2: Illustration of the factor graph and the message passing algorithm for  $q_X$ .

where  $\alpha_t$  and  $\beta_t$  are the well known forward and backward messages corresponding to forward and backward filtering. The marginal moments of  $\mathbf{x}_t$  and  $(\mathbf{x}_t, \mathbf{x}_{t+1})$  are defined by

$$q_X(\mathbf{x}_t, \mathbf{x}_{t+1}) \propto \Psi_{t,t+1}(\mathbf{x}_t, \mathbf{x}_{t+1}) \alpha_t(\mathbf{x}_t) \beta_{t+1}(\mathbf{x}_{t+1}) \prod_j \lambda_{t+1,j}^0(x_{t+1}^j),$$

$$q_X(x_{t+1}^j) \propto \psi_{t+1,j}(x_{t+1}^j) \lambda_{t+1,j}^l(x_{t+1}^j).$$

The factor graph and the message passing algorithm corresponding to the model (11) are illustrated in Figures 2 and 3.

Unfortunately, due to the non-Gaussian nature of  $\psi_{t+1,j}$  the messages are not analytically tractable and we have resort to approximate messages to be able to carry out the computations. To deal with the non-Gaussianity of  $\psi_{t+1,j}$  we make use of the form of  $q_X(x_{t+1}^j)$  and  $\lambda_{t+1,j}^0(x_{t+1}^j)$ : we multiply both sides of (12) by  $\lambda_{t+1,j}^l(x_{t+1}^j)$  and define the Gaussian message  $\lambda_{t+1,j}^0(x_{t+1}^j)$  as

$$\lambda_{t+1,j}^0(x_{t+1}^j)^{new} \lambda_{t+1,j}^l(x_{t+1}^j) = \text{Project}[\psi_{t+1,j}(x_{t+1}^j) \lambda_{t+1,j}^l(x_{t+1}^j); \mathcal{N}], \quad (15)$$

where  $\text{Project}[p(\mathbf{x}); \mathcal{N}]$  stands for projection of a distribution  $p(\mathbf{x})$  into the Gaussian family  $\mathcal{N}$  in the moment matching Kullback-Leibler sense, that is,

$$\text{Project}[p(\mathbf{x}); \mathcal{N}] = \underset{q \in \mathcal{N}}{\text{argmin}} D[p(\mathbf{x}) || q(\mathbf{x})].$$

This results in approximate marginals  $\tilde{q}_X(\mathbf{x}_t, \mathbf{x}_{t+1})$  and  $\tilde{q}_X(x_{t+1}^j)$  for which the weak consistency  $\text{Project}[\tilde{q}_X(x_{t+1}^j); \mathcal{N}] = \int d\mathbf{x}_t d\mathbf{x}_{t+1}^j \tilde{q}_X(\mathbf{x}_t, \mathbf{x}_{t+1})$  holds. Since the newly defined  $\lambda_{t+1,j}^0(x_{t+1}^j)$  is Gaussian, the computations for the forward and backward messages in (13) and (14) become tractable.

Note that the method operates by approximating the marginal distributions resulting from the message passing and not the messages themselves. This approach was used in various models and settings such as in hybrid graphical models (Lauritzen, 1996; Heskes and Zoeter, 2002), the cavity method (statistical physics) in Gaussian process regression (Opper

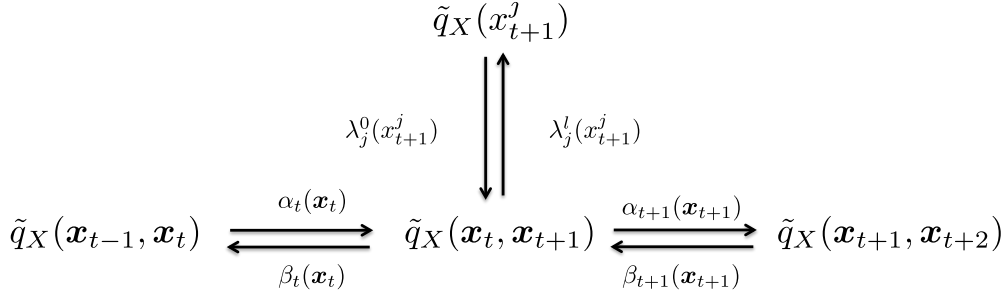


Figure 3: Illustration of the approximate message passing algorithm for  $q_X$ .

and Winther, 2000) and assumed density filtering based factor graph inference (Minka, 2001). Since the message passing is not exact, we have to run it as a fixed point iteration over the messages. Similarly to most convergent fixed point algorithms, the iteration typically converges fast and provides good quality approximations (e.g. Kuss and Rasmussen, 2005). Its relation to the state of the art machine learning methods will be discussed in Section 3.1.3. Further details and references about convergence are given in the Supplementary Material.

### 3.1.1 Exploiting sparsity

Although the above approximate messages make the message passing algorithm tractable— $\alpha_t$ ,  $\beta_t$ ,  $\lambda_{t+1,j}^0$  and  $\lambda_{t+1,j}^l$  become Gaussian—, in case of large state spaces the  $O(n^3)$  storage and computational costs can become unmanageable. On the other hand, we notice that due to the structural sparsity of  $\mathbf{A}$  and  $\mathbf{Q}$ , the precision structure of the Gaussian term  $\Psi_{t,t+1}(\mathbf{x}_t, \mathbf{x}_{t+1})$  can also be sparse. This sparsity however, is “destroyed” when the contribution of the forward and backward messages  $\alpha_t$  and  $\beta_{t+1}$  with full precision matrices, is added, see (13) and (14). Thus the marginalisation required to compute  $\alpha_{t+1}$  and  $\beta_t$ , in its current form, cannot make use of sparsity. It then makes sense to restrict the precision structure of the Gaussian messages  $\alpha_t(\mathbf{x}_t)$  and  $\beta_{t+1}(\mathbf{x}_{t+1})$  to arrive at a sparse precision structure for  $\tilde{q}_X(\mathbf{x}_t, \mathbf{x}_{t+1})$ . This would allow us to use fast sparse linear algebraic methods such as sparse Cholesky factorisation and partial matrix inversion to compute the required moments. Later on, we show that due to the properties of these linear algebraic methods, the messages can be computed efficiently and that all moments required for updating  $q_{AZ}$  and  $q_Q$  can be computed even if we use restricted messages.

Let  $\mathbf{f}(\mathbf{z}) = (z_1, \dots, z_n, \{-z_i z_j / 2\}_{i \sim j})$  denote the sufficient statistic of a Gaussian Markov random field where  $i \sim j$  follows the connectivity of a graph  $G(\mathbf{f})$ . We use  $\text{Project}[p(\mathbf{z}); \mathcal{N}_{\mathbf{f}}]$  to denote the Kullback-Leibler moment matching projection to the Gaussian family defined by  $G(\mathbf{f})$ , that is,  $\text{Project}[p(\mathbf{z}); \mathcal{N}_{\mathbf{f}}]$  is the Gaussian distribution  $q(\mathbf{z})$  with precision structure  $G(\mathbf{f})$  that minimises  $D[p(\mathbf{z}) || q(\mathbf{z})]$ .

By multiplying (13) and (14) with the corresponding  $\beta_{t+1}$  and  $\alpha_t$  messages and making

use of the form of  $\tilde{q}_X(\mathbf{x}_t, \mathbf{x}_{t+1})$ , we define the (approximate) message updates

$$\alpha_{t+1}(\mathbf{x}_{t+1})^{new} \beta_{t+1}(\mathbf{x}_{t+1}) \propto \text{Project} \left[ \int d\mathbf{x}_t \tilde{q}_X(\mathbf{x}_t, \mathbf{x}_{t+1}); \mathcal{N}_{\mathbf{f}} \right] \quad (16)$$

$$\beta_t(\mathbf{x}_t)^{new} \alpha_t(\mathbf{x}_t) \propto \text{Project} \left[ \int d\mathbf{x}_t \tilde{q}_X(\mathbf{x}_t, \mathbf{x}_{t+1}); \mathcal{N}_{\mathbf{f}} \right] \quad (17)$$

$$\lambda_{t+1,j}^l(x_{t+1}^j)^{new} \lambda_{t+1,j}^0(x_{t+1}^j) \propto \text{Project} \left[ \int d\mathbf{x}_t d\mathbf{x}_{t+1}^{\setminus j} \tilde{q}_X(\mathbf{x}_t, \mathbf{x}_{t+1}); \mathcal{N} \right]. \quad (18)$$

This ensures that the forward and backward messages  $\alpha_t$  and  $\beta_t$  have a sparse precision structure  $G(\mathbf{f})$  at all times. The message passing algorithm has to be run iteratively until a fixed point is reached. Once convergence is achieved, the above definition of the messages results in the weak consistency conditions

$$\text{Project} \left[ \int d\mathbf{x}_{t-1} \tilde{q}_X(\mathbf{x}_{t-1}, \mathbf{x}_t); \mathcal{N}_{\mathbf{f}} \right] = \text{Project} \left[ \int d\mathbf{x}_{t+1} \tilde{q}_X(\mathbf{x}_t, \mathbf{x}_{t+1}); \mathcal{N}_{\mathbf{f}} \right].$$

In the following section we detail the computational issues related to the newly introduced approximate message passing: (1) we show that fast linear algebraic methods can be applied to exploit sparsity, (2) we detail when and under which conditions on  $G(\mathbf{f})$  we can define an efficient message passing algorithm, and show that (3) inference with restricted messages can indeed provide the necessary moment parameters to define  $q_{AZ}$  and  $q_Q$  and thus run the (approximate) structured variational optimisation.

### 3.1.2 The $\text{Project}[\cdot; \mathcal{N}]$ operations

The  $\text{Project}[q_X(x_{t+1}^j); \mathcal{N}]$  step in (15) can be performed as follows. Since  $\psi_{t+1,j}$  depends only on  $x_{t+1}^j$ , we have to compute the first and second moments of  $z$ , where  $z$  is distributed according to an un-normalised distribution  $\psi_{t+1,j}(z) \times \exp(hz - qz^2/2)$ , with  $h$  and  $q$  being the canonical parameters in  $\lambda_{t+1,j}^l$ . Since the computation of the moments cannot be carried out analytically, one has to resort to numerical approximations. We propose two alternatives: (i) applying Gauss-Hermite numerical quadrature w.r.t.  $z$  or (ii) finding the Gaussian approximation of  $\psi_{t+1,j}(z) \exp(hz - qz^2/2)$  by the univariate Laplace method and performing Gauss-Hermite numerical quadrature w.r.t. this approximation. Because of the univariate Newton method we use, method (ii) is slightly more computationally expensive than method (i), however, it is more accurate when the masses of  $\psi_{t+1,j}(z)$  and  $\exp(hz - qz^2/2)$  are far apart as it is often the case in the first few updates. Due to the accuracy of these univariate methods, the numerical error in computing the moments and thus  $\text{Project}[\tilde{q}_X(x_{t+1}^j); \mathcal{N}]$  is negligible.

The  $\text{Project}[\int d\mathbf{x}_t d\mathbf{x}_{t+1}^{\setminus j} \tilde{q}_X(\mathbf{x}_t, \mathbf{x}_{t+1}); \mathcal{N}]$  step in (18) reduces to the computation of the marginal means and variances of  $\mathbf{x}_{t+1}$  in  $\tilde{q}_X(\mathbf{x}_t, \mathbf{x}_{t+1})$ . This requires a marginalisation which can be computationally expensive. The crucial idea that leads to significant computational savings is that, in order to preserve sparsity, we carry out the computations on the joint  $\tilde{q}_X(\mathbf{x}_t, \mathbf{x}_{t+1})$  by using sparse partial matrix inversion via sparse Cholesky factorisation and solving the corresponding Takahashi equations (Takahashi et al., 1973). Let  $(\mathbf{h}_{\alpha_t}, \mathbf{Q}_{\alpha_t})$  and  $(\mathbf{h}_{\beta_{t+1}}, \mathbf{Q}_{\beta_{t+1}})$  denote the canonical parameters of the messages  $\alpha_t$  and  $\beta_{t+1}$ , and let us concatenate the parameters of  $\lambda_{t+1,j}^0$  into the representation  $(\mathbf{h}_{\lambda_{t+1,j}^0}, \mathbf{Q}_{\lambda_{t+1,j}^0})$  where, due to the



univariate nature of the message  $\lambda_{t+1,j}^0$  the precision parameter  $\mathbf{Q}_{\lambda_{t+1,\cdot}^0}$  is diagonal. With this notation, the precision matrix of  $\tilde{q}_X(\mathbf{x}_t, \mathbf{x}_{t+1})$  can be written as

$$\mathbf{Q}_{t,t+1} = \begin{bmatrix} \langle \mathbf{A}^T \mathbf{Q} \mathbf{A} \rangle_{q_{AZ} q_Q} + \mathbf{Q}_{\alpha_t} & -\langle \mathbf{A} \rangle_{q_{AZ}}^T \langle \mathbf{Q} \rangle_{q_Q} \\ -\langle \mathbf{Q} \rangle_{q_Q} \langle \mathbf{A} \rangle_{q_{AZ}} & \langle \mathbf{Q} \rangle_{q_Q} + \mathbf{Q}_{\beta_{t+1}} + \mathbf{Q}_{\lambda_{t+1,\cdot}^0} \end{bmatrix}. \quad (19)$$

The sparsity of  $\mathbf{Q}_{t,t+1}$  is governed by the sparsity of  $\mathbf{A}^T \mathbf{Q} \mathbf{A}$  and the sparsity of the messages' precision structure  $\mathbf{Q}_{\alpha_t}$  and  $\mathbf{Q}_{\beta_{t+1}}$ . To compute the required moments we (i) solve the system  $[\mathbf{Q}_{t,t+1}]^{-1}[\mathbf{h}_{t,t+1}]$ , where  $\mathbf{h}_{t,t+1}^T = [\mathbf{h}_{\alpha_t}^T, \mathbf{h}_{\beta_{t+1}}^T + \mathbf{h}_{t+1}^{y^T} + \mathbf{h}_{\lambda_{t+1,\cdot}^0}^T]$  and (ii) compute the diagonal of  $[\mathbf{Q}_{t,t+1}^0]^{-1}$ . We do this by a sparse Cholesky factorisation of a convenient reordering of  $\mathbf{Q}_{t,t+1}$  followed by (i) solving triangular sparse linear systems and (ii) doing a partial inversion by solving the Takahashi equations (Takahashi et al., 1973). Let  $\mathbf{L}\mathbf{L}^T = [\mathbf{Q}_{t,t+1}]_{\sigma,\sigma}$  where  $\sigma$  is the permutation corresponding to a reordering. Then the partial inversion using the Takahashi equations computes all entries of  $[[\mathbf{Q}_{t,t+1}]_{\sigma,\sigma}]^{-1}$  for which  $\mathbf{L}$  is non-zero. This implies that all entries of  $[\mathbf{Q}_{t,t+1}]^{-1}$  where  $\mathbf{Q}_{t,t+1}$  is non-zero are computed (Davis, 2006). This is a property which is further exploited in the  $\text{Project}[\cdot; \mathcal{N}_f]$  step. The partial matrix inversion can be viewed as running a junction tree algorithm on the Gaussian graphical model defined by  $\mathbf{Q}_{t,t+1}$ , where the junction tree is constructed during the sparse Cholesky factorisation (Davis, 2006).

The  $\text{Project}[\cdot; \mathcal{N}_f]$  steps in (16) and (17) computing the temporal messages  $\alpha_{t+1}$  and  $\beta_t$  can be performed as follows. Let  $q(\mathbf{x}) = N(\mathbf{x}|\mathbf{m}, \mathbf{V})$ , then  $\text{Project}[q(\mathbf{x}); \mathcal{N}_f]$  (see Section 3.1.1) simplifies to solving

$$\begin{aligned} \underset{\hat{\mathbf{Q}}}{\text{minimise}} \quad & \text{tr}(\mathbf{V}\hat{\mathbf{Q}}) - \log \det \hat{\mathbf{Q}} \\ \text{s.t.} \quad & \hat{Q}_{i,j} = 0, \text{ for all } (i,j) \notin G(\mathbf{f}), \end{aligned}$$

and computing  $\hat{\mathbf{h}} = \hat{\mathbf{Q}}^{-1}\mathbf{m}$ . The optimisation can be solved by gradient based methods or the Newton method and the calculations are computationally expensive. However, when the graph  $G(\mathbf{f})$  is chordal (e.g. Lauritzen, 1996), the optimality conditions lead to equations that can be solved exactly (instead of expensive optimisation) by using the values  $\mathbf{V}_{ij}$  with  $(i,j) \in G(\mathbf{f})$  (Dahl et al., 2008). Since the covariance values corresponding to the non-zeros in  $\mathbf{Q}_{\alpha_t}$  and  $\mathbf{Q}_{\beta_{t+1}}$  are all already computed by the partial matrix inversion of  $\mathbf{Q}_{t,t+1}$ , no further covariance computations are needed to perform the required projection. For this reason, we use restricted temporal messages where  $G(\mathbf{f})$  is chordal.

For chordal  $G(\mathbf{f})$ s the equations for the optimality conditions can be solved as follows, see (Dahl et al., 2008) for further details. Assume further that the cliques  $C_1, \dots, C_K$  of the  $G(\mathbf{f})$ 's junction tree are ordered such that if  $C_i$  is an ancestor of  $C_j$  then  $i \leq j$ . Let  $S_j = C_j \cap (C_1 \cup C_2 \cup \dots \cup C_{j-1})$  and  $R_j = C_j \setminus (C_1 \cup C_2 \cup \dots \cup C_{j-1})$ . Then  $\hat{\mathbf{Q}} = (\mathbf{I} + \mathbf{U})\mathbf{D}(\mathbf{I} + \mathbf{U})^T$ , where  $\mathbf{U}$  and  $\mathbf{D}$  can be computed iteratively from

$$\mathbf{U}_{R_k, S_k} = -\mathbf{V}_{S_k, S_k}^{-1} \mathbf{V}_{S_k, R_k}, \quad (20)$$

$$\mathbf{D}_{R_k, R_k} = [\mathbf{V}_{R_k, R_k} - \mathbf{V}_{R_k, S_k} \mathbf{V}_{S_k, S_k}^{-1} \mathbf{V}_{S_k, R_k}]^{-1}. \quad (21)$$

The computational complexity scales with  $\sum_k \max\{|S_k|^3, |R_k|^3, |S_k|^2|R_k|\}$ . The size of the cliques depends on the structure of  $G(\mathbf{f})$ . See Section 3.1.4 for further details.



In the last two sections we detailed the technicalities of local computations in the message passing algorithm and have shown how we can exploit sparsity by making use of the properties of sparse linear algebraic methods and of probabilistic inference in Gaussian graphical models (e.g. [Lauritzen, 1996](#); [Davis, 2006](#)). In the following we address the scheduling of message passing and the choice of the sparsity structures of  $G(\mathbf{f})$ .

### 3.1.3 Message passing schedules

The choice of  $G(\mathbf{f})$ , and the scheduling of the updates in the fixed point iteration in (15)-(18) govern the accuracy and the computational complexity of the inference algorithm. In the following we detail our choices and show how some of them are related to methods available in the current literature.

Based on the complexity of  $\text{Project}[:, \mathcal{N}_f]$  we consider three main classes for  $G(\mathbf{f})$ : (i) *full*, where  $G(\mathbf{f})$  is fully connected, this corresponds to the EP style approximate inference approach of propagating full Gaussian messages (ii) *chordal*, where  $G(\mathbf{f})$  is a chordal graph, corresponding to messages having precision matrices with restricted sparsity structure, and (iii) *diag*, where  $G(\mathbf{f})$  is a disconnected graph, corresponding to factorised temporal messages, that is, only marginal means and variances are propagated.

In terms of scheduling we differentiate the following choices: (i) *static*, where the forward backward updates (16)-(17) are iterated until convergence and then the (15) and (18) updates are performed, (ii) *sequential*, where the (15) and (18) updates are iterated until convergence followed by the corresponding (16)-(17) updates, and (iii) *dynamic*, where in order to minimise the number of update steps, we use greedy scheduling strategy to be detailed later. Note that in all cases the (15) and (18) updates are performed for all  $j$  at once; this corresponds to the so called parallel EP scheduling in [Gerven et al. \(2009\)](#) and [Cseke and Heskes \(2011\)](#).

$G(\mathbf{f})$  is *fully connected (full)*. In this case both  $\mathbf{Q}_{\alpha_t}$  and  $\mathbf{Q}_{\beta_t}$  are full matrices implying that the diagonal blocks of  $\mathbf{Q}_{t,t+1}$  are full and thus we are no longer dealing with sparse matrices. However, the *sequential* version of this algorithm corresponds to the approximate filtering-smoothing approach with EP approximations for the non-Gaussian terms. The *static* version of this algorithm can be shown to be a version of expectation propagation in a block Gaussian model: the Gaussian forward-backward message passing corresponds to computing the marginal means and variances needed for the (15) and (18) updates. Compared to the Gaussian EP presented in [Cseke and Heskes \(2011\)](#), the difference is in the (15) step: here we use forward-backward message passing to compute the moments needed for (18) while the method in [Cseke and Heskes \(2011\)](#) corresponds to applying sparse partial matrix inversion to an  $n \times T$  sized sparse matrix. Due to this connection, the approximation provided by the latter two methods are identical. For large  $ns$  (few hundreds or thousands) and  $T$ s (few hundreds), however, both can become excessively demanding.

$G(\mathbf{f})$  is *partially connected (chordal, tsp)*. The *chordal* case is computationally less intensive than the *full* because it can preserve sparsity. This is both due to the sparsity of  $\mathbf{Q}_{\alpha_t}$  and  $\mathbf{Q}_{\beta_{t+1}}$ , and of  $\mathbf{Q}_{t,t+1}$ . The computational cost of (16) and (17) is much less than the  $O(n^3)$  complexity of the *full* case. A special chordal case is when  $G(\mathbf{f})$  is a tree. In this case the complexity of  $\text{Project}(:, \mathcal{N}_f)$  is  $O(n)$ . A plausible choice is the maximum weight spanning tree of  $|\mathbf{A}|$ , we call this *tsp*. We detail the choice of chordal graphs in Section 3.1.4,

however, typically one can assume that the computational complexity of the partial matrix inversion of  $\mathbf{Q}_{t,t+1}$  and the collapse operations scales as  $O(n^2)$ , that is, in the worst case we expect  $O(\sqrt{n})$  cliques of size  $O(\sqrt{n})$  in the corresponding junction trees. Operating on sparse matrices results in significant gains in terms of computing time. Although one expects that due to the “less informative” messages more update steps might be needed, there is a very significant overall gain in speed as shown in Section 4. This clearly comes at the price of obtaining approximations that are less accurate than in case of *full*, however in many large scale applications this loss is not very significant and one ends up with an overall advantageous compromise. The *static* scheduling option can be viewed as replacing the forward-backward type partial inversion to compute the marginal means and variances with an approximate (faster) forward-backward algorithm. In the *sequential* and *dynamic* scheduling cases we have very significant computational gains, since the linear algebraic operations are now carried out on sparse matrices.

$G(\mathbf{f})$  is *disconnected (diag)*. This case corresponds to the inference scheme where the temporal messages are factorised. When  $G(\mathbf{f})$  is disconnected,  $\mathbf{Q}_{\alpha_t}$  and  $\mathbf{Q}_{\beta_{t+1}}$  are diagonal, therefore, the temporal messages add no computational cost.  $\text{Project}[\cdot; \mathcal{N}_{\mathbf{f}}]$  simplifies to identifying marginal means and variances, that is, it is the same as  $\text{Project}[\cdot; \mathcal{N}]$  in (18). As a result, the partial matrix inversion of  $\mathbf{Q}_{t,t+1}$  is very fast and  $\text{Project}[\cdot; \mathcal{N}_{\mathbf{f}}]$  comes at no computational cost. The computational cost scales with that of a sparse Cholesky factorisation and thus scales as  $O(n \log(n)^3)$ . The *static* and *sequential* scheduling strategies have the same properties as in the *chordal* case.

*Dynamic scheduling and distributed computing.* The computation is dominated by the number of partial matrix inversions of  $\mathbf{Q}_{t,t+1}$  and ideally, in all inference schemes, we would like to design a message-passing algorithm that achieves convergence by using the least possible number of partial inversion. Clearly, this is not a straightforward problem to solve. For this reason, we propose a greedy *dynamic* scheduling where at every step we select the message that has the largest (last) update (in terms of canonical parameters), and update both the receiver and the source of this message be it either  $\tilde{q}_X(\mathbf{x}_t, \mathbf{x}_{t+1})$  or  $\tilde{q}_X(x_{t+1}^j)$ . This is implemented by (i) keeping track of the updates in each  $\alpha_t, \beta_t, \lambda_{t+1,j}^0$  and  $\lambda_{t+1,j}^l$  and (ii) updating all outgoing messages when updating an approximate marginal density. The computational saving due to the greedy *dynamic* scheduling are shown on the right panel of Figure 11. Alternative measures such as change in KL divergence or in moments can be used to choose the marginals to be updated.

By constructing longer scheduling queues (ranking the change in messages, instead of choosing the maximal change) one can distribute the computation to several processing units and achieve a further reduction of computing time. We distribute the computation by selecting and scheduling locally independent receiver-source pair updates to different computational cores. This leads to significant speedups compared to the traditional forward-backward type algorithms that are sequential by definition. We adapted the greedy approach by greedily selecting as many disjunct receiver-source pairs from the message error ranking as the number of computational units. Currently, we can achieve a five fold reduction in computation time using eight processing cores in our Matlab<sup>2</sup> implementation. We believe that this can be further improved by fine-tuning our ranking and scheduling scheme and by

---

<sup>2</sup><http://www.mathworks.com>

making better use of Matlab’s distributed computing toolbox.

### 3.1.4 Chordal $G(\mathbf{f})$ s and row-column permutations

The computing time/complexity is dominated by the partial inversion of  $\mathbf{Q}_{t,t+1}$ . The complexity of the computation is determined by the choice of  $G(\mathbf{f})$ . As detailed in Sections 3.1.2 and 3.1.3 the structure of  $\mathbf{Q}_{t,t+1}$  can range from full in case of *full* to a minimally sparse structure in case of *diag*. In this section we motivate our choices of chordal  $G(\mathbf{f})$ s. We start from the intuition that  $G(\mathbf{f})$ s that reflect the spatial connectivity (finite element grid structure) of the model would be good candidates for the precision structure of the messages. Note, that as shown in Section 2 and illustrated in Figure 1, this grid structure is identical to the sparsity structure  $S(\mathbf{A})$  of the state transition matrix  $\mathbf{A}$ . Unfortunately,  $S(\mathbf{A})$  is typically not a chordal graph. In order to define a chordal  $G(\mathbf{f})$ , we propose to complete  $S(\mathbf{A})$  to a chordal graph by adding the least possible number of additional entries (edges in  $G(\mathbf{f})$  or the triangular grid). These additional edges might not have direct intuitive meaning in terms of the model structure, however, their use enables efficient inference and minimises the computation time.

It is well known that the sparse Cholesky factorisation creates sparsity structures that correspond to chordal graphs and that the structure of these graphs, as well as the number of additional, so called, “fill in” edges depend on the row-column permutations or reordering methods applied prior to the factorisation (Davis, 2006). The sparsity structure of the Cholesky factor is computed before any numerical evaluations take place (symbolic Cholesky factorisation). Depending on the sparsity structure of the matrix to be factorised, various row-column permutations have been proposed to minimise the number of “fill-in”s. We make use of these properties of the factorisation to complete  $S(\mathbf{A})$  to a chordal graph. Suppose  $\sigma$  is a permutation, to be chosen later, and that  $S(\mathbf{L})$  is the symbolic Cholesky factor of  $S(\mathbf{A}_{\sigma,\sigma})$ . Then we use the chordal graph  $G(\mathbf{f}) = [S(\mathbf{L}) + S(\mathbf{L}^T)]_{\sigma^{-1},\sigma^{-1}}$  to define the precision structure of the temporal messages. There are several well-known “fill-in” reducing reordering permutations. In this paper we use (i) the approximate minimum degree (**amd**) permutation, (ii) the symmetric reverse Cuthill-McKee (**rcm**) permutation, and (iii) the nested dissection (**nd**) permutation (Davis, 2006).

When performing the Cholesky factorisation and partial matrix inversion of  $\mathbf{Q}_{t,t+1}$ , we consider the same permutations. We do an empirical estimation of the computational cost of the (18) as well as the (16)-(17) steps and we choose the best performing pair of permutations for  $S(\mathbf{A})$  and  $\mathbf{Q}_{t,t+1}$ . In the models we considered, the best performing pairs were the **amd** and **nd** permutations to obtain  $G(\mathbf{f})$ —from  $S(\mathbf{A})$ —and **amd** for the factorisation and partial inversion of  $\mathbf{Q}_{t,t+1}$ . The latter operation typically dominated the computing time and **amd** outperformed the other methods. **amd** and **nd** led to structures in  $G(\mathbf{f})$  that resulted in similar computing times in the  $\text{Project}[\cdot; \mathcal{N}_{\mathbf{f}}]$  step (similar clique size distribution, see Section 3.1.2). If none of the above mentioned or any other chordal completion strategies are satisfactory or the structures in the model allow faster alternative methods, one can revert to a different  $G(\mathbf{f})$  and perform the  $\text{Project}[\cdot; \mathcal{N}_{\mathbf{f}}]$  as most appropriate in his/her model’s context.

The panels of Figure 4 visualise the sparsity structures of  $G(\mathbf{f})$ ,  $\mathbf{Q}_{t,t+1}$  and the corresponding Cholesky factor for various choice of reordering permutations. The matrix  $\mathbf{A}$

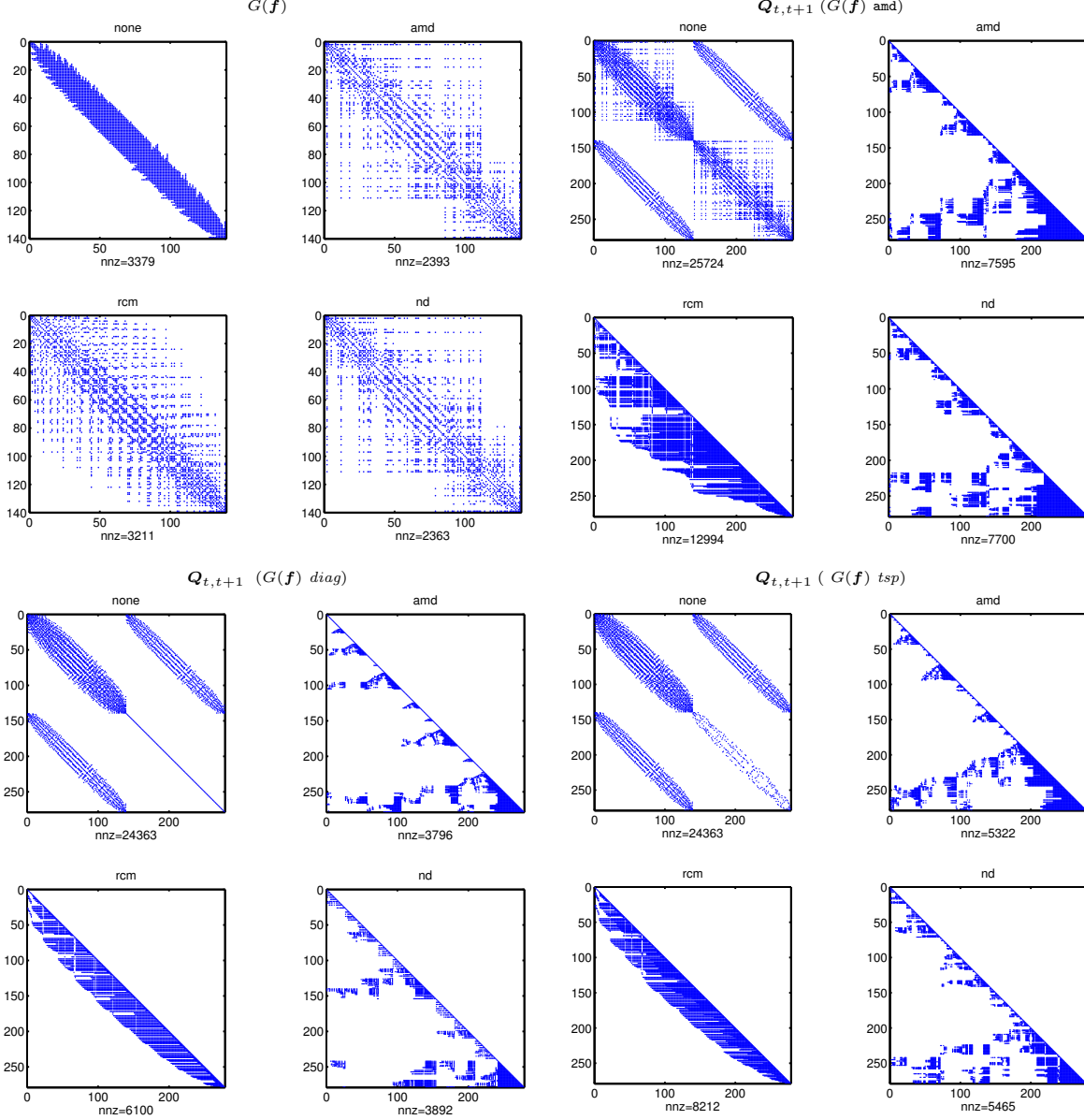


Figure 4: Illustration of the sparsity structures of the matrices  $G(\mathbf{f})$  and  $Q_{t,t+1}$  on a grid model similar to the one in Figure 1. The panels in the  $G(\mathbf{f})$  block show the chordal completions of the sparsity structure of the grid and thus of  $\mathbf{A}$  obtained by symbolic Cholesky factorisations using "fill-in" reducing permutations. The rest of the panels show the structure of  $Q_{t,t+1}$  for the corresponding choice of  $G(\mathbf{f})$  (top-left) as well as the structure of Cholesky factors for various reordering permutations applied to  $Q_{t,t+1}$ .

corresponds to a grid structure similar to that in Figure 1 and  $Q$  is chosen to be diagonal. The  $G(\mathbf{f})$  group of panels show that the lack of reordering generates a significantly less sparse  $G(\mathbf{f})$ s than the ones using reordering. The *amd* and *nd* permutation generate  $G(\mathbf{f})$ s with a similar number on non-zero elements. The rest of the panels show the structure of  $Q_{t,t+1}$ s

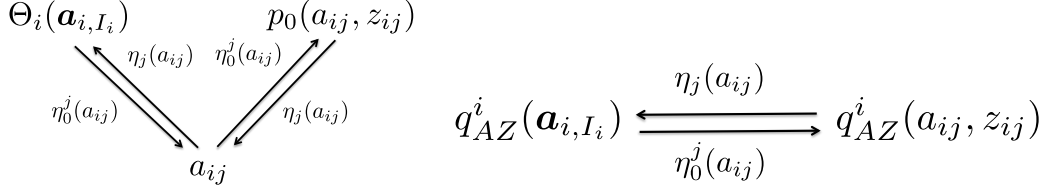


Figure 5: Illustration of the factor graph and the corresponding message passing algorithm for  $q_{AZ}^i$ .

(labeled none) and their corresponding Cholesky factors for corresponding to **amd**, **rcm**, and **nd** permutations. Note that  $S(\mathbf{A})$  is shown on the off-diagonal block of the  $\mathbf{Q}_{t,t+1}$  panels.. The **amd** and **nd** permutations applied to  $\mathbf{Q}_{t,t+1}$  lead to a similar number of non-zero elements in the Cholesky factor. Note that *diag* leads to structures that are significantly sparser and the average number of non-zeros per column in the factor is much smaller than in any other case. This has a significant impact on the performance of the partial matrix inversion by the Takahashi equations which scale as  $\sum_j (\sum_{i:L_{i,j} \neq 0} 1)^2$  (Takahashi et al., 1973).

### 3.2 The model $q_{AZ}$

In this section we present the inference method for the elements of the transition matrix  $\mathbf{A}$  as well as their relevance  $\mathbf{Z}$ . In this paper we are interested in learning dynamics for models with diagonal  $\mathbf{Q}$ , therefore, we only present the inference for such models. The method for general  $\mathbf{Q}$ s is presented in the Supplementary Material. For diagonal choices of  $\mathbf{Q}$ , the distribution  $q_{AZ}$  factorises as  $q_{AZ}(\mathbf{A}, \mathbf{Z}) = \prod_i q_{AZ}^i(a_{i,I_i}, z_{i,I_i})$  (see (9) in Section 2) and the resulting graphical models or factor graphs are tree structured or more specifically, star structured. Note that due to the sparse grid structure the cardinality of  $I_i$  is typically low, say 6 – 10, and exact inference can be done in reasonable time.

Let  $\prod_i \Theta_i(\mathbf{a}_{i,I_i}) \propto \exp\{\sum_i \langle \log p(\mathbf{x}_{t+1}|\mathbf{x}_t, \mathbf{A}, \mathbf{Q}) \rangle_{q_X, q_Q}\}$  denote the Gaussian terms resulting from taking expectations w.r.t.  $q_X$  and  $q_Q$ . We can then write  $q_{AZ}^i$  as

$$q_{AZ}^i(\mathbf{a}_{i,I_i}, \mathbf{z}_{i,I_i}) \propto \Theta_i(\mathbf{a}_{i,I_i}) \prod_{j \in I_i} p_0(a_{ij}|z_{ij})p(z_{ij}). \quad (22)$$

We can then write the (exact) message passing algorithm by introducing the messages  $\eta_j(a_{ij})$  and  $\eta_0^j(a_{ij})$ ,  $j \in I_i \cup \{0\}$ , respectively such that

$$\begin{aligned} \eta_j(a_{ij}) &\propto \sum_{z_{ij}} p_0(a_{ij}|z_{ij})p(z_{ij}) \quad \text{for all } j \in I_i \\ \eta_0^j(a_{ij}) &\propto \int d\mathbf{a}_{i, \setminus j} \Theta_i(\mathbf{a}_{i,I_i}) \prod_{k \in I_i \setminus \{j\}} \eta_j(a_{ik}). \end{aligned}$$

In the first equation we sum out the variables  $z_{ij}$  and thus the messages  $\eta_j(a_{ij})$  are mixtures of Gaussians, while in the second equation we compute the marginals w.r.t.  $a_{ij}$  of the thus newly created  $|I_i|$  dimensional Gaussian mixture with  $2^{|I_i|}$  components. The factor graph and

the message passing corresponding to the model (22) is illustrated in Figure 5. We can use  $q_{AZ}^i(a_{ij}, z_{ij}) \propto p_0(a_{ij}|z_{ij})p(z_{ij})\eta_0^j(a_{ij})$  to compute the marginal distribution of the variables  $z_{ij}$  whereas the marginals of  $\mathbf{a}_{i,I_i}$  can be computed from  $q_{AZ}^i(\mathbf{a}_{i,I_i}) = \Theta_i(\mathbf{a}_{i,I_i}) \prod_{k \in I_i \setminus \{j\}} \eta_j(a_{ik})$ .

The first and second moments of  $\mathbf{a}_{i,I_i}$  needed to update  $q_X$  are computed from  $q_{AZ}^i(\mathbf{a}_{i,I_i})$ , whereas  $q_{AZ}^i(z_{ij})$  can be used to measure the relevance of  $a_{ij}$ . In the cases when  $\mathbf{Q}$  is not diagonal the model for  $q_{AZ}$  is larger and exact inference is intractable. Therefore, we have to resort to the approximate message passing. The form of this non-factorising model and the corresponding message passing are given in the Supplementary Material.

### 3.3 The model $q_Q$

In general we choose conjugate priors for  $\mathbf{Q}$  or we keep it fixed. When  $\mathbf{Q}$  is diagonal, as it is the case in most real life models we address, the free form expression in (10), together with our model definition, shows that  $q_Q$  factorises as  $q_Q(\mathbf{Q}) = \prod_i q_Q(q_{ii})$  and that due to conjugacy, the marginals  $q_Q(q_{ii})$  are gamma distributed. Moreover, the variables  $q_{ii}$  are only present in  $q_X$  and the necessary moments to be computed are only the first moments  $\langle q_{ii} \rangle_{q_Q}$ .

## 4 Experiments

In this section we assess the speed and accuracy of the inference methods we introduced and show the potential use of this approach in the WikiLeaks Afghan War Diary data studied in Zammit-Mangion et al. (2012a). The algorithms have been coded in Matlab and we use the partial matrix inversion algorithm of Gerven et al. (2012) which is implemented in the C programming language.

### 4.1 Accuracy of state space inference in 1D models

In this section we assess the accuracy of the state space inference methods in 1D Gaussian and Poisson models. We use the Gaussian model to assess the accuracy of restricted (temporal) message passing inference such as *diag*, *chordal*, while the Poisson model will be used to assess the accuracy of the inference methods in non-Gaussian models.

#### 4.1.1 Models and accuracy measures

In both cases we consider a diffusion model on a 1D grid with  $n - 1$  grid intervals ( $n$  state space variables,  $\mathbf{x}_t \in \mathbb{R}^n$ ) and  $T$  time points. We define  $\mathbf{A}$  as a symmetric banded matrix with various bandwidths  $n_{\text{neighb}}$  and  $A_{ij} = (1 - \epsilon_{\mathbf{A}})/(1 + 2n_{\text{neighb}})$  (values for nodes close to the boundaries are rescaled accordingly to obtain a constant row-sum  $1 - \epsilon_{\mathbf{A}}$ ). We define the system noise's inverse covariance  $\mathbf{Q}$  as a linear combination of a first order intrinsic field's precision matrix and a unit diagonal matrix. We introduce a parameter  $s$  to control the correlation decay in  $\mathbf{Q}^{-1}$  and normalise  $\mathbf{Q}$  to obtain a chosen variance value  $v_x$ . Formally,  $\mathbf{Q}$  is defined as

$$\mathbf{R}(s) = \mathbf{I} + 10^s \mathbf{R}_1 \quad \text{and} \quad \mathbf{Q}(v_x, s) = v_x^{-1} \sqrt{\text{diag}(\mathbf{R}(s)^{-1})} \mathbf{R}(s) \sqrt{\text{diag}(\mathbf{R}(s)^{-1})},$$



where  $\mathbf{R}_1$  denotes the tridiagonal precision corresponding to  $\sum_i (x_{i+1} - x_i)^2$  and  $\text{diag}(\mathbf{R}(s)^{-1})$  is the diagonal matrix formed by the diagonal of  $\mathbf{R}(s)^{-1}$ . The left panel of Figure 6 show how  $s$  influences the correlation decay.

The observation models are defined as follows. In the Gaussian case we assume that we observe the field with an observation noise variance  $v_{\text{obs}}$  and that the field is only partially observed: we sample the locations of the observations from the  $n \times T$  space-time grid uniformly with probability  $p_{\text{obs}}$ . In the Poissonian case the observations are Poisson random numbers with a mean  $\exp\{x_t^i\}$  and we sample at all locations of the space-time grid.

As mentioned above, in the Gaussian case we focus on the accuracy of *diag* and *chordal*—*full* being exact—to assess the loss of accuracy due to the restricted temporal messages. Since the paradigm behind the state space inference method is to approximate the two time slice marginals  $\tilde{q}_{t,t+1}(\mathbf{x}_t, \mathbf{x}_{t+1})$ , the accuracy measure we choose is the symmetric KL divergence w.r.t. the exact two time slice marginals  $p_{t,t+1}(\mathbf{x}_t, \mathbf{x}_{t+1})$  computed by *full*. Therefore, we define the accuracy measure

$$S(\{p_{t,t+1}\}_t, \{\tilde{q}_{t,t+1}\}_t) = \frac{1}{2(T-1)} \sum_{t=1}^{T-1} \left\{ D[\tilde{q}_{t,t+1} \| p_{t,t+1}] + D[p_{t,t+1} \| \tilde{q}_{t,t+1}] \right\}. \quad (23)$$

In the Poissonian case the quality of the approximation is affected both by the restricted temporal messages and the non-Gaussian nature of the problem. In the previous section we highlighted that the message exchange with the non-Gaussian likelihood terms is in fact a locally performed expectation propagation algorithm. It is well known that this expectation propagation performs very well on models with non-Gaussian likelihood terms similar to the Poisson distribution (stochastic volatility models, log-Gaussian Cox models), see for example (Zoeter and Heskes, 2005; Cseke and Heskes, 2011). Thus our aim here is to asses the joint effect of both sources of inaccuracy.

In the Gaussian case the KL measure seems to be a reasonable choice to assess the distributional accuracy. However, in the Poissonian case there is no exact method to compare to, therefore, we opt for the quantile-quantile (Q-Q) plots as a basis to measure accuracy. Since the accuracy measure should reflect the local nature (we only approximate marginals) of the algorithm, we use the local Gaussian approximation  $\tilde{q}_{t,t+1}(\mathbf{x}_t, \mathbf{x}_{t+1})$  to compute the normalised residuals  $\hat{\mathbf{x}}_{t,t+1}$  w.r.t. the state space values  $\tilde{\mathbf{x}}_{t,t+1}$  used in the data generation. Formally, we define the residuals as

$$\hat{\mathbf{x}}_{t,t+1} = \mathbf{L}_{t,t+1}^T (\tilde{\mathbf{x}}_{t,t+1} - \mathbf{m}_{t,t+1}),$$

where  $\mathbf{m}_{t,t+1}$  and  $\mathbf{Q}_{t,t+1} = \mathbf{L}_{t,t+1} \mathbf{L}_{t,t+1}^T$  are the mean and precision corresponding to  $\tilde{q}_{t,t+1}(\mathbf{x}_t, \mathbf{x}_{t+1})$ . We then use the quantile values to assess how well the elements of  $\hat{\mathbf{x}}_{t,t+1}$  (when aggregated to a single set) obey the standard normal distribution. We use the mean absolute deviation from the standard normal quantiles as accuracy measure.

#### 4.1.2 Experiments

In the Gaussian case we consider models with  $n_x = 64$ ,  $T = 100$  and  $n_{\text{neighb}} \in \{1, 2, 4, 8\}$ . We choose a system noise variance  $v_{\text{sys}} = (0.5)^2$ , an observation noise variance  $v_{\text{obs}} = (0.25)^2$  and we set  $p_{\text{obs}} = 0.75$ . We choose  $s \in \{-1, 0, 1\}$  leading to the correlation functions shown on the left panel of Figure 6. We simulate the models starting from the corresponding steady state

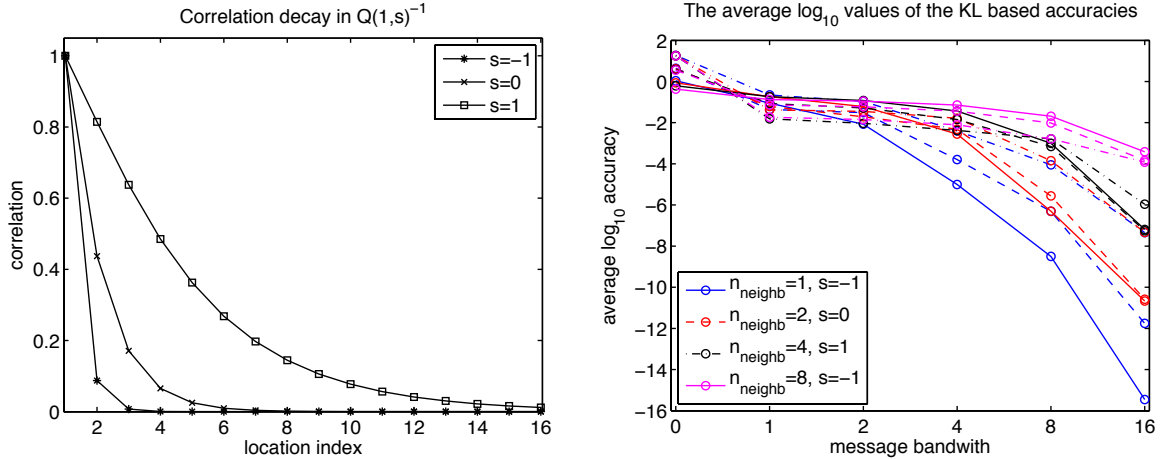


Figure 6: Quantifying accuracy for the 1D Gaussian model. The left panel shows the correlation decay in  $Q(v_x, s)^{-1}$  w.r.t. the variable index  $i$  in  $x_t^i$  for  $s \in \{-1, 0, 1\}$  while the right panel shows the average over  $n_{\text{exp}} = 25$  runs of the log of KL accuracy score (23) for various choices of  $n_{\text{neighb}}$  (colour) and  $s$  (line style).

conditions. All these parameter choices together with  $\epsilon_A = 0.025$  lead to simulated samples with rich variations in the latent field  $\{x_t\}_t$  in the given time window. We simulated  $n_{\text{exp}} = 25$  runs for each model and we computed the KL based score in (23) for *diag* ( $n_{\text{msg}} = 0$ ) and for the *chordal* models corresponding to messages with bandwidths  $n_{\text{msg}} \in \{1, 2, 4, 8, 16\}$  in their precision matrix, thus varying the accuracy of the approximation. Note that  $n_{\text{msg}} = 64$  corresponds to the exact *full* method and due to the univariate nature of the problem, all chordal methods (*amd*, *nd* and *rcm*) lead to the same structure in the temporal messages' precision matrix. For each inference method, the inference scheme was run until the change in the maximum absolute value in the message parameters became smaller than  $10^{-8}$ . The right panel of Figure 6 shows the average log KL accuracies w.r.t. the message bandwidth  $n_{\text{msg}}$  for various choices of  $n_{\text{neighb}}$  and  $s$ . The accuracy plots show that for the *diag* method ( $n_{\text{msg}} = 0$ ) the accuracy is dominated by  $s$  and that the chordal methods lead to a very significant improvement in accuracy. The general pattern in the variation of the accuracy w.r.t.  $n_{\text{neighb}}$  and  $s$  is that smaller correlation in  $Q^{-1}$  and fewer neighbours in  $A$  lead to better accuracy. For all cases the accuracy increases as the message bandwidth  $n_{\text{msg}}$  increases thus validating the usefulness of the *chordal* inference methods.

In the Poissonian case we used the same latent diffusion model, generated Poisson observations—see the left panel of Figure 7—and used the same inference schemes and stopping criteria as in the Gaussian case. For each run we measured the accuracy of the inference by computing the mean deviation of the quantile-quantile curve from the diagonal—we used 50 quantile bins. We then averaged these quantities over the  $n_{\text{exp}} = 25$  experiments for each choice of  $n_{\text{neighb}}$ ,  $s$  and message bandwidth  $n_{\text{msg}}$ . The values are shown in the right panel of Figure 7. The plots show that similarly to the Gaussian case, the quality of the approximation improves as we increase the message bandwidth  $n_{\text{msg}}$  and that, typically, there is a significant increase in accuracy when moving from *diag* to *chordal* methods. As in the Gaussian case, the weaker the diffusion (smaller  $n_{\text{neighb}}$ ) the more accurate the method is,



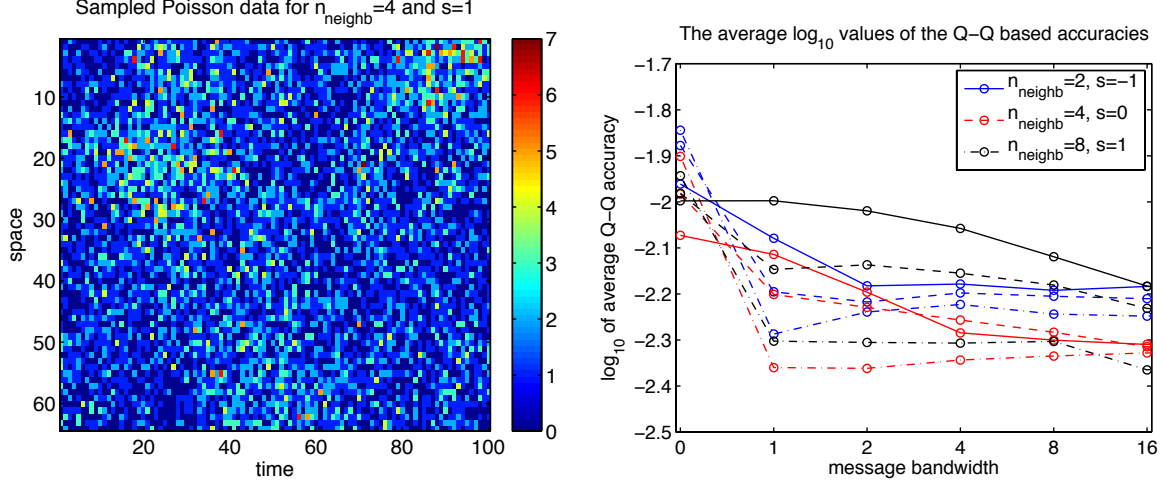


Figure 7: Quantifying accuracy for the 1D Poisson model. The left panel shows sampled Poisson data from the model while the right panel shows the logarithm of the average (over  $n_{\text{exp}} = 25$  runs) mean quantile deviations (50 bins) for various choices of  $n_{\text{neighb}}$  (colour) and  $s$  (line style).

however, it seems that in this case correlation in  $\mathbf{Q}^{-1}$  leads to slightly improved accuracy whenever it can be captured well—see the performance of the *chordal* methods over the *diag* one and the bad performance of diagonal for  $s \in \{0, 1\}$ .

## 4.2 Accuracy and structure recovery in a 2D spatial model

In this section we consider a two dimensional spatio-temporal model where we vary the transition matrix  $\mathbf{A}$  and a diagonal inverse covariance  $\mathbf{Q}$  and we assess the accuracy of the state space inference and the recovery rate of the network structure corresponding to  $\mathbf{A}$ . In order to obtain interesting dynamics, we define the field on a circular domain and choose the structure of the matrix  $\mathbf{A}$  such that the model gives rise to a rotating “motion” in the Gaussian field. To achieve this, we define  $\mathbf{A}$  as follows: we start from a symmetric structure given by a triangular grid and for each node  $i$  we eliminate all incoming edges  $(i, j)$  that form a negative vector product with the radius at the location of node  $i$ . We then set the elements of the  $i$ -th row of  $\mathbf{A}$  according to

$$A_{ii} = w \quad \text{and} \quad A_{ij} = (1 - \epsilon_w - w)/|\delta(i)| \text{ for all } j \in \delta(i).$$

We set  $\epsilon_w$  to a small value such that the row  $\mathbf{A}_{i,\cdot}$  sums lower than 1 resulting in a zero stationary mean value for the state space. We set  $\epsilon_w = 0.05$ . The top left panel in Figure 8 illustrates the transition matrix  $\mathbf{A}$  constructed in this way and the rest of the panels show samples from the field  $z_t(s) = \sum \phi_i(s)x_t^i$  and the event data generated from it. We vary the diagonal values of  $\mathbf{A}$  by choosing  $w \in [0, 1]$  and vary the system noise  $\mathbf{Q}^{-1} = \sigma^2 \mathbf{I}$  by choosing  $\sigma^2 \in \{0.5, 1, 2\}$ . The stationary mean and covariance of  $\{\mathbf{x}_t\}$  are given by

$$\mathbf{m}_\infty = \mathbf{A}\mathbf{m}_\infty \quad \text{and} \quad \mathbf{V}_\infty = \mathbf{A}\mathbf{V}_\infty\mathbf{A}^T + \sigma^2 \mathbf{I}$$

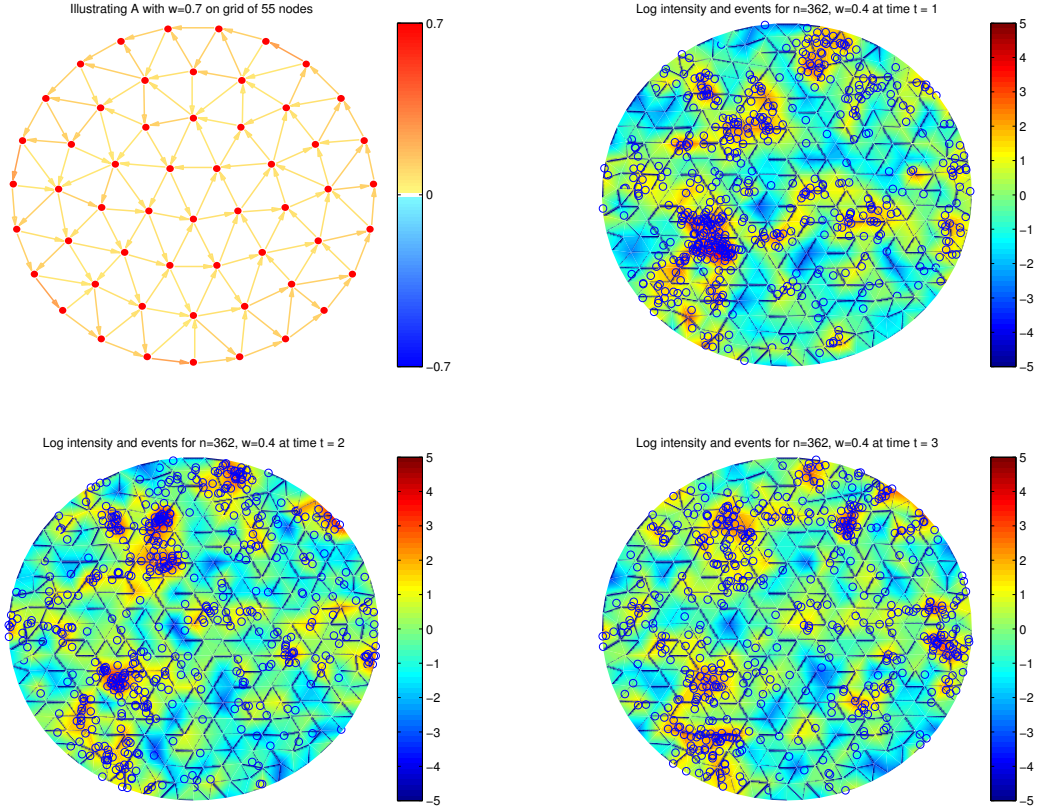


Figure 8: The top left panel shows the transition matrix  $\mathbf{A}$  for a 2D model with  $w = 0.7$  and a state space size  $n_x = 55$ . The rest of the panels show the log intensity and the sampled events corresponding to a sequence of 3 steps from a model with  $n_x = 362$ ,  $w = 0.4$  and  $\sigma^2 = 1$  and a similarly structured transition matrix as in the top left panel. The resulting field, and consequently the point patterns, exhibit a rotation motion.

and thus the mean value of the stationary intensity reads as

$$\langle \lambda_\infty(\mathbf{s}) \rangle = \exp \left\{ \boldsymbol{\phi}(\mathbf{s})^T \mathbf{m}_\infty + \frac{1}{2} \boldsymbol{\phi}(\mathbf{s})^T \mathbf{V}_\infty \boldsymbol{\phi}(\mathbf{s}) \right\},$$

where  $\boldsymbol{\phi}(\mathbf{s})^T = [\phi_1(\mathbf{s}), \dots, \phi_n(\mathbf{s})]^T$  stands for the local linear basis defined by the triangular grid. We simulate artificial event data by using initial samples from the stationarity distribution. The mean  $\mathbf{m}_\infty$  is typically sufficiently close to zero to be negligible, thus the mean intensity is determined by  $\mathbf{V}_\infty$ , that is, by  $w$  and  $\sigma^2$ . In the first experiment we assess how the accuracy of the state space inference varies in terms of  $w$  and  $\sigma^2$ , while in the second one we fix  $\sigma^2 = 1$  and do joint inference for the parameter  $\mathbf{A}$  and the state space  $\mathbf{X}$ .

We assess the accuracy of the state space inference on models with  $n \in \{362, 1008\}$ . We generate a sequence of  $T = 50$  state space samples  $\{\tilde{\mathbf{x}}_t\}$  starting from the stationary phase and sample the event data by using a standard thinning method. We then run the state space inference methods using the  $w$  and  $\sigma^2$  parameters the data was generated by. The panels in Figure 9 show the Q-Q plots for various settings of  $w$  and  $\sigma^2$ . We can see that on this model the methods have very similar performance (the Q-Q plots overlap) and there is a decrease in performance as the values of  $w$  and  $\sigma^2$  increase. The overlap of the Q-Q plots can be explained by the diagonal nature of  $\mathbf{Q}$  (low noise correlation) and the magnitude of the Q-Q accuracies—see Section 4.1.2. The worsening of performance due to increasing  $w$ -s is negligible compared to that of  $\sigma^2$  which can be explained by the fact that higher system noise leads to less accurate approximations.

Recovering the structure of  $\mathbf{A}$  is important in many spatio-temporal applications where we want to infer how the occurrence of events spreads over a certain geographic area, see for example the data in Section 4.4. As we already mentioned, we start from the connectivity structure defined by the triangular grid and infer the elements of  $\mathbf{A}$  given this assumption. To test the edge recovery, we generate data by using the above described construction of  $\mathbf{A}$  and a fixed  $\sigma^2 = 1$ , and infer the (approximate) posterior distribution of  $\mathbf{X}$ ,  $\mathbf{A}$  and  $\mathbf{Z}$ . Note that we infer the posterior distribution of  $\mathbf{A}$  where we assume that  $\mathbf{A}$  has the same prior structure as the grid, and not the posterior distribution of  $w$ . In Section 3 we mentioned that the (approximate) posterior distribution of the variables  $z_{ij}$  can be used to quantify the relevance of an edge  $(i, j)$ . Here we use  $p(z_{ij} = 1)$  as classification scores to assess whether the correct edges have been eliminated from the prior grid structure, that is  $p(z_{ij} = 1)$  will be used as a score for  $A_{ij} \neq 0$ . We construct receiver-operator curves (ROC) to assess the quality of the structure inference. The ROCs and the area under these curves are widely used in machine learning as a method to assess classification performance. The panels in Figure 10 show the ROC curves for various choices of  $w$ ,  $T$  and approximation methods. We can conclude that, as expected, the quality of the recovery increases as  $T$  increases for all values of  $w$ . It is interesting to get a confirmation that lower values of  $w$  and thus higher diffusion speeds lead to better performance on structure recovery in a limited time window. The difference in various state space inference methods is hardly noticeable in these models and is well within the expected statistical variation. This lack of significant difference can be explained by the accuracy results discussed in the previous section (high accuracy in state space inference).

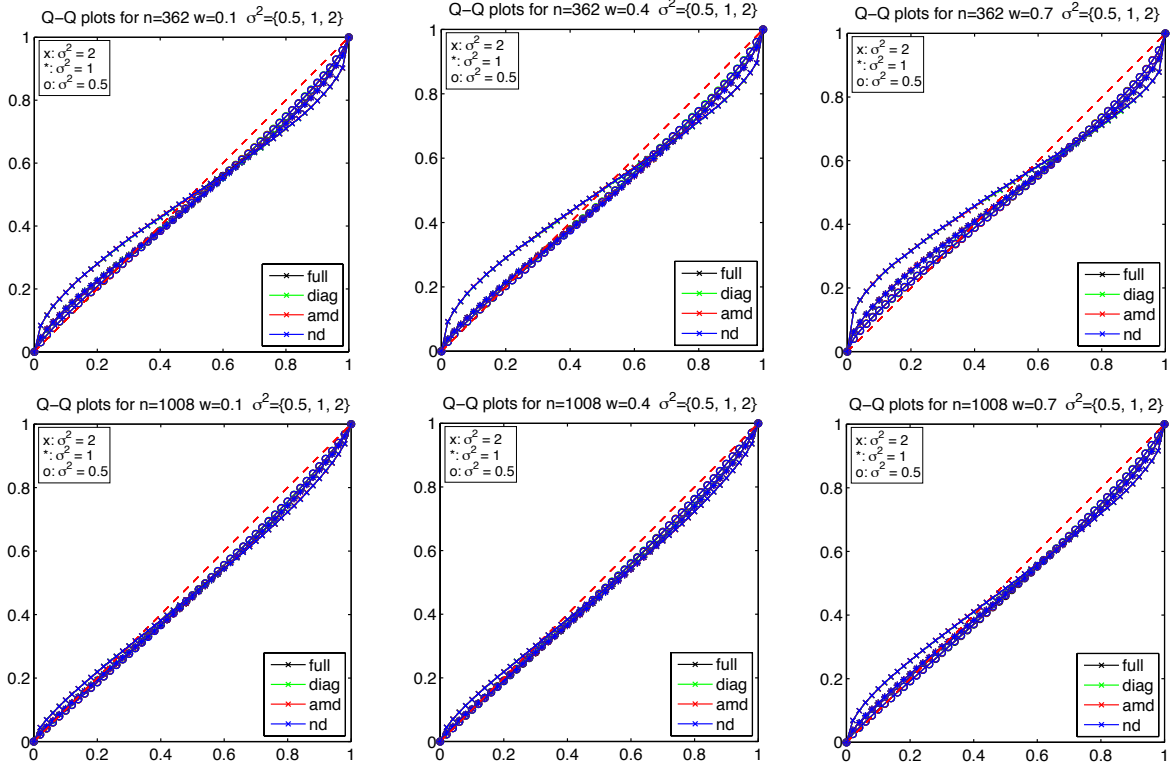


Figure 9: Accuracy of the state space approximation in a 2D spatial model. The panels show the Q-Q plots for a variety of parameter settings and methods in models with  $n = 362$  (top) 1008 (bottom) and  $T = 50$ . The plots were generated by assessing how well the sampled path fits to the posterior state space approximation, see Section 4.2.

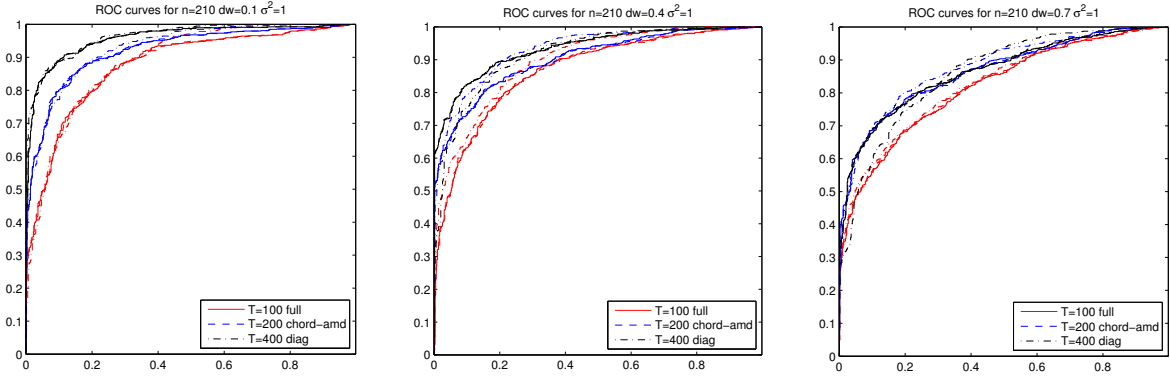


Figure 10: Structure recovery. The panels of the figure show the receiver ROCs for various settings of  $w$  and  $T$  for a variety of state space inference methods, see Section 4.2. Colours denote the choices of  $T$ , line types denote the inference method used for  $q_X$ .

### 4.3 Running times and scalability

To compare running times, we choose a typical scenario where the latent field is governed by

$$\begin{aligned} dz(\mathbf{s}, t) &= \mathcal{A}z(\mathbf{s}, t)dt + dW(\mathbf{s}, t), \\ z(\mathbf{s}, 0) &= z_0(\mathbf{s}), \end{aligned} \tag{24}$$

with  $W(\mathbf{s}, t)$  being a space-time Wiener process having a covariance operator  $\Sigma u(\mathbf{s}) = \int k(\mathbf{s}, \mathbf{r})u(\mathbf{r})d\mathbf{r}$ . The operator  $\mathcal{A} = D\Delta(\cdot)$ , where  $\Delta(\cdot)$  is the Laplacian and we use again a circular domain with radius  $r$ . Temporal discretisation with  $\Delta_t = 0.01$  followed by the Galerkin method in conjunction with a row-sum lumping method (Bueche et al., 2000; Lindgren et al., 2011) was applied to obtain a sparse matrix  $\mathbf{A}$  with  $n = 2267$  for simulating data. We used  $T = 200$  time points. We set  $r = 10, D = 0.2$  and assumed that the discretised precision matrix  $\mathbf{Q}$  is diagonal with elements  $1/15$ . We obtain diagonal  $\mathbf{Q}$ s when using the covariance function  $k(\mathbf{s}, \mathbf{r}) = \sum_i \phi_i(\mathbf{s})\phi_i(\mathbf{r})\tilde{\lambda}_i = \phi(\mathbf{s})^T \mathbf{\Lambda} \phi(\mathbf{r})$ . We found that under this configuration, at stationarity, around 1000 points per time frame were generated; a typical count for large data sets.

The algorithms were tested on Delaunay triangulations of the domain constructed using routines by Persson and Strang (2004) with varying mesh density,  $n \in \{362, 562, 1008\}$ . Computing times were recorded using Matlab’s profiler. The message passing was run until a message accuracy of  $10^{-4}$ . To ensure a fair comparison, all test results given here are with computations restricted to a single processor core.<sup>3</sup>

The computing times for the sequential scheduling are plotted in the left panel of Figure 11. We segmented the computing times to correspond to the three main operations: (1) *temporal messages* stands for the max determinant optimisation problem (overhead in *full*) (2) *overhead* accounts for initialisations, updating messages and monitoring convergence (3) *lin- $\text{alg}$*  logs the time for linear algebraic operations (Cholesky factorisation, partial matrix inversion), and (4) *non-Gaussian* stands for the univariate moment computations to update  $\lambda_{t,j}^0$ . For clarity, we omit results for the static case which were up to an order of magnitude slower than the second worst-performing method. This slow performance is attributed to the number of iterations required for convergence, which is typically more than the number of forward-backward cycles required by the *full*.

The left panel in Figure 11 shows that, for small  $n$ , the *full* inference scheme is faster than the other schemes due to the fact that it is implemented more efficiently in terms of matrix operations (Matlab/LAPACK core routines). However, the situation changes for large  $n$  and for  $n = 1008$ , where we see that the *full* is slower than the best *chordal* methods and much slower than the *tsp* and *diag*. Note that the increase in computing time is well below cubic and at most quadratic for all methods other than the *full*.

Significant speed-ups are possible when using greedy scheduling (see right panel in Figure 11). Although the scheduling itself does not affect the scalability of the algorithm, it can be seen that, as expected, the greedy scheduling can reduce the computing time. For instance, after the initial forward-backward, the *full* needed only a few factor updates to achieve convergence within tolerance.

---

<sup>3</sup>All algorithms were tested on an Intel Core™i7-2600S @ 2.80GHz personal computer with 8GB of RAM.

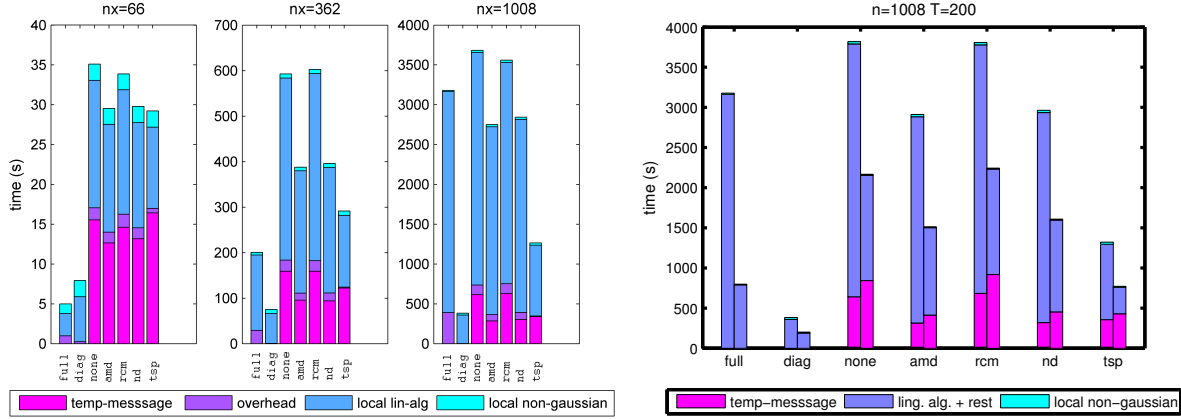


Figure 11: Running times for various state space sizes and scheduling options. (left) Running times for the inference schemes *full*, *diag*, and chordal schemes *none*, *amd*, *rcm*, *nd* and *tsp* (left panel). Comparison in terms of running times of the sequential (left bar) and greedy (right bar) scheduling strategies. Local operations refer for the local linear algebra whilst the temporal messages refer to the max-determinant optimisation (right panel).

## 4.4 The Afghan War Diary

Spatio-temporal point-process methods have been recently shown to be a valuable tool in the study of conflict. In [Zammit-Mangion et al. \(2012b\)](#), a dynamic spatio-temporal model, inspired by the integro-difference equation, was used to obtain a posterior estimates of conflict intensity in Afghanistan and to predict conflict levels using an iterative state-parameter update scheme on the WikiLeaks Afghan War Diary (AWD). Updates on  $\mathbf{x}_t$  were found using an algorithm similar to the *full* described above. The spatial scales considered there were on the order of a 100 km and thus, modelling of micro-scale effects such as relocation or escalation diffusions in conflict were not possible. Conflict dynamics are known to occur at much smaller scales ([Schutte and Weidmann, 2011](#)), even at resolutions of  $\approx 10$  km. The goal of this section is thus primarily to show that we can perform inference at such high resolutions and, in addition, estimate the dynamics on the required spatial and temporal scales.

### 4.4.1 State estimation using fixed parameters

The aim of this example is to show that we can carry out state inference at scale by inferring conflict intensity in space and time for the entire density. Afghanistan has an area of over 500000 km<sup>2</sup> and the WikiLeaks data set contains over 70000 events. The mesh we employed (using population density as a proxy for mesh density), shown in [Figure 12](#) has the largest triangles with sides of 22km and the smallest ones with sides of 7km. The total number of vertices amounts to  $n = 9398$  in a system with  $T = 313$  time points (weeks).

We constructed  $\mathbf{A}$  from the diffusion equation above with  $D = 1 \times 10^{-4}$  with latitude/longitude used as spatial units.  $\mathbf{Q} = 0.2 \times \mathbf{I}$  was taken as rough value from the full joint analysis using a low resolution model, see [Zammit-Mangion et al. \(2012a\)](#) for details. We carried out inference in the AWD with the *diag* algorithm, which took only a few hours on a standard PC and consumed only about 4GB of memory. The considerable performance



achieved implies that, with appropriate exploitation of clustered/distributed computational resources, full state-parameter inference of very large systems can be carried out in considerably shorter timescales and with potentially less resources than previously envisioned.

A characteristic plot showing one week of the conflict progression (first week of October 2009) is given in Figure 12. At this point, in the conflict activity in the south in Helmand and Kandahar was reaching its peak and conflict at the Pakistani border was intensifying considerably. The insets show how detailed inferences can be made - note that here we have employed fixed hyper-parameters; spatially-varying smoothness as in (Lindgren et al., 2011) may be introduced even in this simple model with relative ease.

#### 4.4.2 Learning conflict dynamics from the AWD

In the context of conflict, the dynamic behaviour of events is usually extracted from the data by gridding the domain of interest in space and time and carrying out an empirical study on the events *per se*, for example by analysing the pattern of boxes which contain at least one event at two consecutive time frames Baudains et al. (2013); Schutte and Weidmann (2011). Unfortunately, due to an explicit reliance on the use of multiple observations to obtain a reliable estimator, these methods are only able to provide global assessments of the dynamics, i.e. assert whether phenomena such as escalation or relocation are present everywhere on average. Here, on the other hand, we can provide spatially-resolved maps of conflict patterns and, moreover, are able to assign a probability to the presence or absence of dynamics.

The most important phenomena considered are containment (events repeat in the same location), escalation (events repeat and also spill into surrounding areas), and relocation (events move from one area to the next). All of these contagion phenomena may be interpreted directly from our posterior beliefs on  $\mathbf{A}$  and the diagonal elements of  $\mathbf{Q}$ . For example, a vertex with low values of  $q_{ii}$  and  $\mathbf{a}_{\cdot,j}$  is indicative of an area where events do occur, but do not escalate or diffuse to surrounding areas. On the other hand large values in  $\mathbf{a}_{i\cdot}$  are indicative of an area that is susceptible to nearby conflict events whilst large values for  $\mathbf{a}_{\cdot,j}$  are indicative of an area that is a large potential contributor to conflict contagion.

The last interpretation is particularly interesting, not only for retrospective analysis and prediction purposes, but also for generating insights into mechanisms which could be employed to contain contagion. One may summarise the role of a region in conflict by summing over the respective columns and rows in  $\mathbf{A}$  (excluding the diagonal elements) in order to obtain a *source* index and a *sink* index respectively for each vertex respectively. The difference between these two indices can then be seen as a measure of how likely a region is to contribute to conflict in the surrounding areas and how likely conflict in a region is *due to* conflict in a neighbouring area.

As a proof of concept, we employ the full model to obtain a map of contagion for Helmand using data between May 2006 and November 2009, shown in Fig. 13. It is beyond the scope of this work to analyse the map in detail, however, three things are of note. First, although not evident from this figure, there is no direct correlation between event intensity and contagion, suggesting that the inference is able to distinguish between containment and relocation/escalation. Second, all airports in the vicinity (three in this case: Kandahar in the South East, Laskar Gah in the South West and Tarin Kowt in the North East) are highlighted

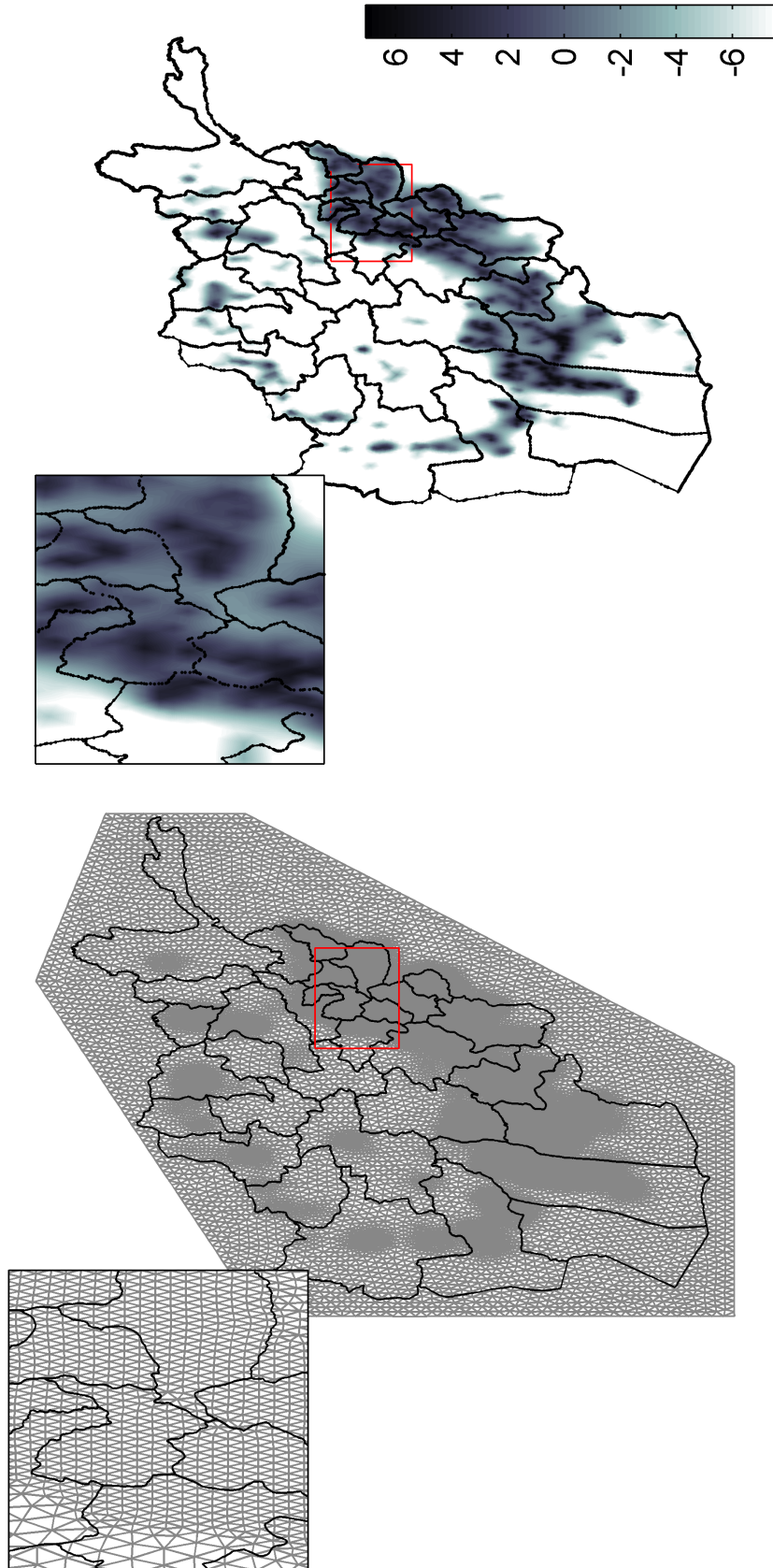


Figure 12: The mesh and one time-slice log intensity map corresponding to the AWD on the first week of October 2009.



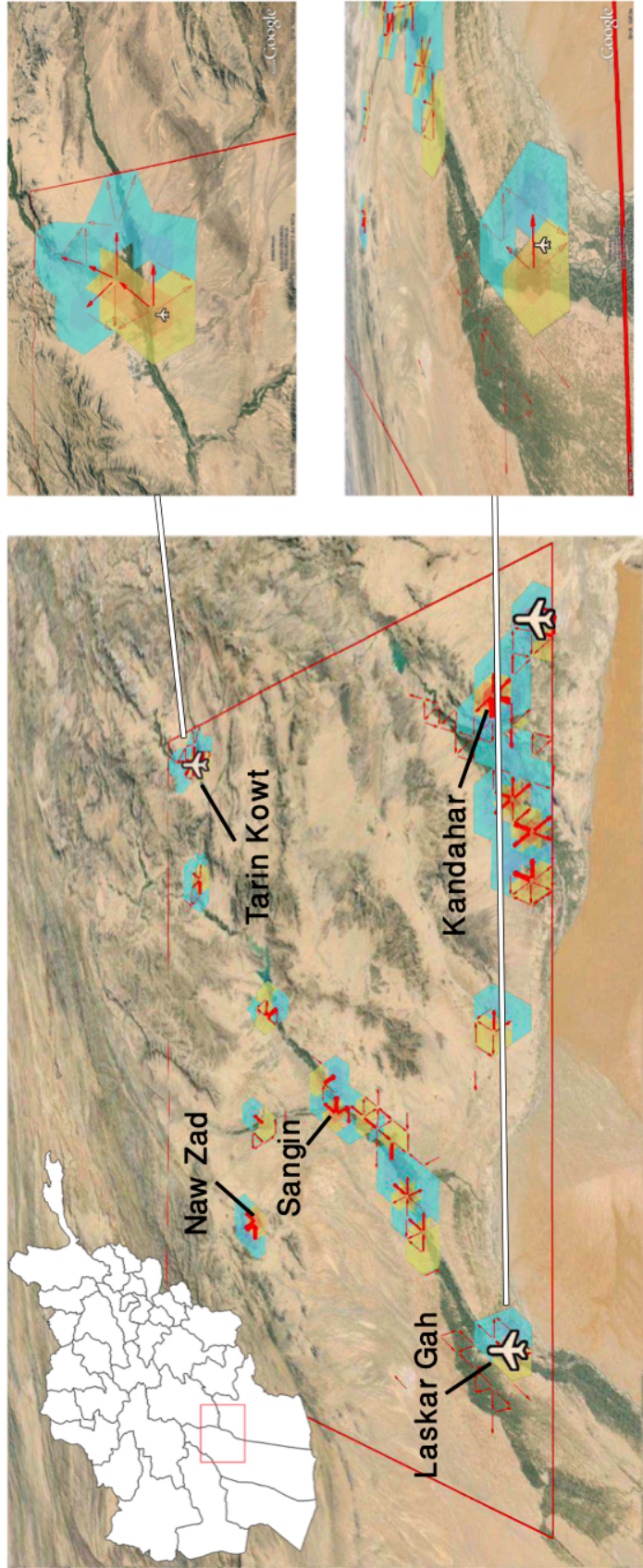


Figure 13: **Left:** The difference between the extent of sourcing (red) and sinking (blue) of conflict event intensity in part of Southern Afghanistan. The aeroplane symbols denote airport locations whilst the arrows denote the relevant edges in  $\mathcal{A}$  with arrow thickness proportional to the element size. **Right:** Insets showing the detail at the airports near Laskar Gah and Tarin Kowt.

as a *source* of conflict, which is not surprising given the strategic importance airbases. Third, several of the source hot spots are on towns and villages which have played a prominent role in the Afghan conflict, these include Naw Zad in the North West, the location of multiple offensive operations by the International Security Assistance Force (ISAF) in the latter part of the conflict and Sangin, one of the most hotly contested towns in the conflict. We note that the interpretation of the inferred dynamics is fully dependent on the spatial and temporal resolutions we employ, and may change for different mesh sizes and temporal discretisations.

To evaluate whether the inferred connectivity in  $\mathbf{A}$  makes any improvement on the approach where the evolution of  $x_t^i$ s are considered independent (diagonal  $\mathbf{A}$ ), we propose to use the one step ahead predictive probabilities. We proceed as follows: we infer  $\mathbf{A}_{\text{conn}}$  using a *chordal* method for state space inference and we also infer  $\mathbf{A}_{\text{indep}}$  by assuming a diagonal  $\mathbf{A}$ ; we then use the mean values  $\langle \mathbf{A}_{\text{conn}} \rangle$  and  $\langle \mathbf{A}_{\text{indep}} \rangle$  to compute the predictive probabilities. Note that in the latter case, the inference completely decouples into independent inference tasks for all  $\{x_t^i\}_t$  and  $A_{ii}$ .

The one step ahead predictive probability at time  $t$  is given by

$$p(\mathcal{Y}_{t+1}|\mathcal{Y}_{1:t}, \mathbf{A}) = \int d\mathbf{x}_{t,t+1} p(\mathcal{Y}_{t+1}|\mathbf{x}_{t+1}) N(\mathbf{x}_{t+1}; \mathbf{A}\mathbf{x}_t, \mathbf{Q}^{-1}) N(\mathbf{x}_t; \mathbf{Q}_{\alpha_t}^{-1}\mathbf{h}_{\alpha_t}, \mathbf{Q}_{\alpha_t}^{-1})$$

where  $\mathbf{h}_{\alpha_t}$  and  $\mathbf{Q}_{\alpha_t}$  denote the canonical parameters of the  $\alpha_t(\mathbf{x}_t)$  forward message corresponding to the filtering algorithm following from our chosen state space inference. Clearly, the above quantity is not tractable, therefore, we use the corresponding evidence approximation—see sequential inference scheme in Section 3.1. The integral itself corresponds to expectation propagation based evidence approximation in latent Gaussian models and is known to be a good quality approximation for a variety of (pseudo) likelihood terms (e.g. Kuss and Rasmussen, 2005; Rasmussen, 2005). Formally similar latent Gaussian models where this evidence approximation is shown to perform excellently are the stochastic volatility or log-Gaussian Cox process models in (e.g. Cseke and Heskes, 2011). The cumulative log values of the one step ahead prediction approximations approximate the log evidence and thus we can also use them to do model comparison. In this way we can assess whether a connected or an independent connectivity model explains the data better. Figure 14 shows how the one step ahead predictions  $p(\mathcal{Y}_{t+1}|\mathcal{Y}_{1:t}, \langle \mathbf{A}_{\text{conn}} \rangle)$  and  $p(\mathcal{Y}_{t+1}|\mathcal{Y}_{1:t}, \langle \mathbf{A}_{\text{indep}} \rangle)$  compare. The plot shows that the corresponding predictive log likelihood ratio is positive for most times and that the overall log likelihood ratio (sum of one step ahead log likelihood ratios) is positive. Therefore, our qualitative conclusions about the benefit of learning micro diffusions are supported by quantitative evidence: the (approximated) predictive performance of the model increases and a connected model is more likely than an independent one. As future work, we intend to focus on areas of high conflict intensity to assess how the learned conflict diffusion varies w.r.t. the spatial resolution of the model.

## 5 Conclusions

We proposed a family of approximate inference methods for spatio-temporal log-Gaussian Cox process models; the algorithms are based on variational approximate inference methods using expectation constraints. Note that the method can be applied to any similar latent Gaussian model (25) with general (pseudo) likelihood  $\tilde{\psi}_{t,i}(x_t^i)$ . We show how the sparsity

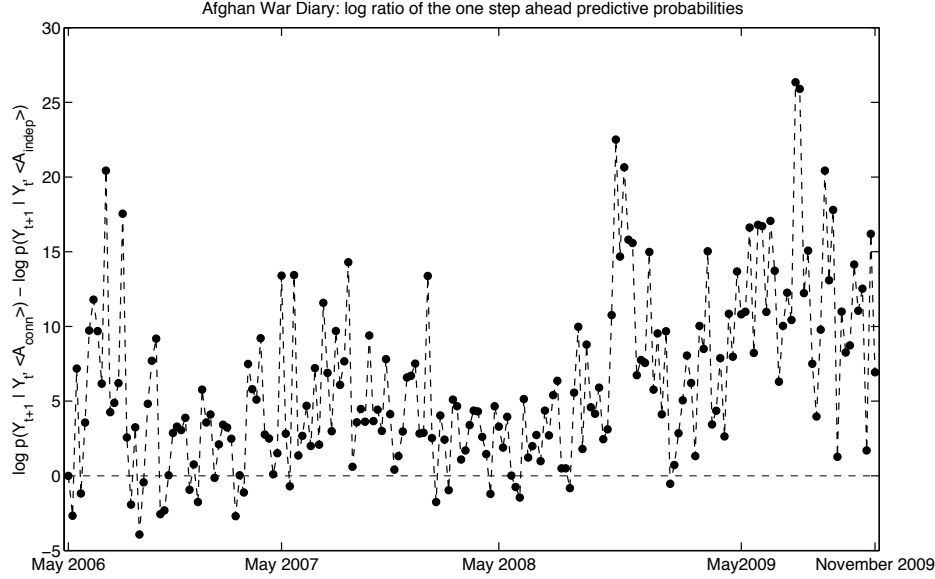


Figure 14: The log ratio of the (approximate) one step ahead predictive probabilities given by the approximations of  $\log p(\mathcal{Y}_{t+1} | \mathcal{Y}_{1:t}, \langle \mathbf{A}_{\text{conn}} \rangle) - \log p(\mathcal{Y}_{t+1} | \mathcal{Y}_{1:t}, \langle \mathbf{A}_{\text{indep}} \rangle)$  for the AWD data. The plot shows that the connected model generally achieves better predictive performance and that the connected model is more likely overall—the sum of log ratios is positive.

in the underlying dynamic model can be exploited in order to overcome the limitations in the standard forward-backward and block inference methods which can become very expensive w.r.t. both storage and computation for large  $n$  and  $T$ . The proposed family of approximate inference schemes provide a wide range of options w.r.t. accuracy and both computational and storage complexity. They are easily adaptable to the computational and storage constraints of the user—for example one can start out with *diag* and move to various *chordal* methods if accuracy needs to be improved. The inference schemes using messages with chordal precision structures can serve as a good compromise in complexity between schemes using diagonal and full precision matrix structures.

We applied the proposed methods to model armed conflict data and we showed that by using the increased resolution resulting from our methods we can detect micro-diffusions in the Afghan War Diary data. By learning these diffusion effects we can improve the predictive performance and obtain plausible qualitative interpretations of conflict spread. The proposed methodology can also be applied to epidemic or environmental studies where sparse latent spatial diffusion models—linear diffusions or linear approximations—can be formulated.

In the future we intend to explore the set of structures that lie between the fast and less accurate spanning tree and the somewhat larger chordal structures employed in this work. Currently, we are working on improving the distributed computing scheduling presented in Section 3.1.3. This is the most important area of further research as the proposed message passing algorithm, by design, is particularly well suited to take advantage of distributed computing environments. However, it is less clear how to distribute computation for the partial inversion (Takahashi equations) needed in the block model. Another notable advantage of our approach, when compared to the block model, is that it more adaptable online settings,

that is, to cases where we have streamed data. We plan to explore this in the future. We expect that dynamic scheduling scheme would be the best suited to do smoothing in online settings.

# Supplementary Material

## Model details

We consider the model defined in the main body of the paper to which we add a set of control variables or covariates  $\{\mathbf{u}_t\}_t, \mathbf{u}_t \in \mathbb{R}^m$  that influence the field  $\{\mathbf{x}_t\}$  through a set of coefficients  $\mathbf{B} \in \mathbb{R}^{n \times m}$ . Thus the model for which we derive the approximate inference can be written as

$$p(\mathcal{Y}, \mathbf{X}, \mathbf{A}, \mathbf{Z}, \mathbf{B}, \mathbf{Q} | \boldsymbol{\theta}, \mathbf{U}) = p_0(\mathbf{x}_1) \prod_t p(\mathbf{x}_{t+1} | \mathbf{x}_t, \mathbf{A}, \mathbf{B}, \mathbf{u}_t, \mathbf{Q}) \prod_j \tilde{\psi}_{t+1,j}(x_{t+1}^j) \quad (25)$$

$$\times \prod_{i \sim j} p_0(a_{ij} | z_{ij}, \boldsymbol{\theta}) p_0(z_{ij} | \boldsymbol{\theta}) \prod_{k,l} p(b_{kl} | \boldsymbol{\theta}) p_0(\mathbf{Q} | \boldsymbol{\theta})$$

with  $\boldsymbol{\theta} = \{\mathbf{m}_1, \mathbf{V}_1, \boldsymbol{\eta}, v_{\text{slab}}, p_{\text{slab}}, v_b, k, \tau\}$  collecting the parameters of

$$\begin{aligned} \tilde{\psi}_{t+1,j}(x_{t+1}^j) &\propto e^{h_j x_{t+1}^j - e^{\eta_j} x_{t+1}^j}, \\ &\propto e^{h_j x_{t+1}^j} \psi_{t+1,j}(x_{t+1}^j) \\ p_0(\mathbf{x}_1) &= N(\mathbf{x}_1; \mathbf{m}_1, \mathbf{V}_1), \\ p(\mathbf{x}_{t+1} | \mathbf{x}_t, \mathbf{A}, \mathbf{B}, \mathbf{u}_t, \mathbf{Q}) &= N(\mathbf{x}_{t+1}; \mathbf{A}\mathbf{x}_t + \mathbf{B}\mathbf{u}_t, \mathbf{Q}^{-1}), \\ p_0(a_{ij} | z_{ij}, \boldsymbol{\theta}) &= N(a_{ij}; 0, z_{ij} v_{\text{slab}}), \\ p_0(z_{ij} | \boldsymbol{\theta}) &= \text{Ber}(z_{ij}; p_{\text{slab}}), \\ p_0(b_{ij} | \boldsymbol{\theta}) &= N(b_{ij}; 0, v_b) \end{aligned}$$

To do approximate inference we start from the free form variational approach. We detail why it is not tractable in its current form and then we present the details of the expectation constraints based procedure.

## 6 Free form variational inference

Here we choose to approximate the joint density  $p(\mathbf{X}, \mathbf{A}, \mathbf{Z}, \mathbf{B}, \mathbf{Q}, |\mathcal{Y}, \mathbf{U})$  with a factorised form  $q_X(\mathbf{X})q_{AZ}(\mathbf{A}, \mathbf{Z})q_B(\mathbf{B})q_Q(\mathbf{Q})$  by using the KL divergence  $D[\cdot || \cdot]$ , that is, we try to solve the optimisation problem

$$\underset{q_X, q_{AZ}, q_Q, q_B}{\text{minimise}} D[q_X(\mathbf{X})q_{AZ}(\mathbf{A}, \mathbf{Z})q_Q(\mathbf{Q})q_B(\mathbf{B}) || p(\mathbf{X}, \mathbf{A}, \mathbf{Z}, \mathbf{Q}, \mathbf{B} | \mathcal{Y}, \mathbf{U})]. \quad (26)$$

The stationarity condition of this minimisation problem yields the structured variational mean field updates

$$[q_x(\mathbf{X})]^{new} \propto \exp \left\{ \langle \log p(\mathbf{X}, \mathbf{A}, \mathbf{Z}, \mathbf{Q}, \mathbf{B} | \mathbf{Y}, \mathbf{U}) \rangle_{q_{AZ} q_Q, q_B} \right\} \quad (27)$$

$$[q_{AZ}(\mathbf{A}, \mathbf{Z})]^{new} \propto \exp \left\{ \langle \log p(\mathbf{X}, \mathbf{A}, \mathbf{Z}, \mathbf{Q}, \mathbf{B} | \mathbf{Y}, \mathbf{U}) \rangle_{q_X q_Q, q_B} \right\} \quad (28)$$

$$[q_Q(\mathbf{Q})]^{new} \propto \exp \left\{ \langle \log p(\mathbf{X}, \mathbf{A}, \mathbf{Z}, \mathbf{Q}, \mathbf{B} | \mathbf{Y}, \mathbf{U}) \rangle_{q_X q_{AZ}, q_B} \right\} \quad (29)$$

$$[q_B(\mathbf{B})]^{new} \propto \exp \left\{ \langle \log p(\mathbf{X}, \mathbf{A}, \mathbf{Z}, \mathbf{Q}, \mathbf{B} | \mathbf{Y}, \mathbf{U}) \rangle_{q_X q_{AZ}, q_Q} \right\} \quad (30)$$

This “coordinate-wise” descend is guaranteed to converge to a local optimum. However, none of the above densities has a tractable form which in turn could be used for computing the required expectations. Due to the form of the model, most of the expectations depend only on marginal densities, therefore, we will use further variational approximate inference techniques to compute accurate approximations. To do this we use an extension of the above variational framework to a variational framework with expectation constraints. We will show that the above structured variational approach and the approximate inference techniques to compute the marginals can be naturally embedded in the same framework. In order to introduce the approximate inference techniques we need to have a closer look at the form of the densities in (27)-(30).

The term that dominates the structure/form of the densities to be approximated is

$$\log N(\mathbf{x}_{t+1} | \mathbf{A}\mathbf{x}_t + \mathbf{B}\mathbf{u}_t, \mathbf{Q}^{-1}) = \frac{1}{2} \log \det(\mathbf{Q}/2\pi) - \frac{1}{2} (\mathbf{x}_{t+1} - \mathbf{A}\mathbf{x}_t - \mathbf{B}\mathbf{u}_t)^T \mathbf{Q} (\mathbf{x}_{t+1} - \mathbf{A}\mathbf{x}_t - \mathbf{B}\mathbf{u}_t). \quad (31)$$

As we can see above, the variational separation of the blocks of variables we choose is well justified: due to the form of the interaction, the joint modelling of the state space and the parameters is problematic as there is hardly any parametric class that could deal with such cases of three-way interactions, whereas when considered conditionally, they are all quadratic. Therefore, the main challenge left to face is how to deal with the non-Gaussian terms and how to scale the inference to large state spaces.

From now on we will use an alternative notation for expectations: an expectation  $h_i(x_i) \equiv \langle h(x_1, \dots, x_i, \dots, x_n) \rangle_{q_1, \dots, q_{i-1}, q_{i+1}, \dots, q_n}$  will also be denoted as  $h_i(x_i) = \langle h(x_1, \dots, x_i, \dots, x_n) \rangle_{\setminus q_i}$ . It will typically be clear from the context what the densities  $q_1, \dots, q_n$  are and which member of the set of densities is omitted.

## 6.1 The model for $q_X$

From (31) we obtain a  $q_x$  that can be rewritten as

$$q_X(\mathbf{X}) \propto \prod_t \Psi_{t,t+1}(\mathbf{x}_t, \mathbf{x}_{t+1}) \prod_j \psi_{t+1,j}(x_{t+1}^j), \quad (32)$$

where  $\Psi_{t,t+1}(\mathbf{x}_{t+1}, \mathbf{x}_t) = \langle \log N(\mathbf{x}_{t+1} | \mathbf{A}\mathbf{x}_t + \mathbf{B}\mathbf{u}_t, \mathbf{Q}^{-1}) \exp\{\mathbf{h}_{t+1} \cdot \mathbf{x}_{t+1}\} \rangle_{\mathbf{q}_X}$  is a canonical Gaussian with parameters  $\langle \mathbf{h}_{t,t+1}^x \rangle_{\mathbf{q}_X}$  and  $\langle \mathbf{Q}_{t,t+1}^x \rangle_{\mathbf{q}_X}$  where

$$\begin{aligned} \mathbf{h}_{t,t+1}^x &= \begin{bmatrix} -\mathbf{A}^T \mathbf{Q} \mathbf{B} \mathbf{u}_t + \delta_0(t, 1) \mathbf{h}_1 \\ \mathbf{h}_{t+1} \end{bmatrix} \\ \mathbf{Q}_{t,t+1}^x &= \begin{bmatrix} \mathbf{A}^T \mathbf{Q} \mathbf{A} + \delta_0(t, 1) \mathbf{Q}_1 & -\mathbf{A}^T \mathbf{Q} \\ -\mathbf{Q} \mathbf{A} & \mathbf{Q} \end{bmatrix}. \end{aligned}$$

Therefore, we have a latent Gaussian model where the non-Gaussian terms depend only on the variables  $x_t^j$ .

## 6.2 The model for $q_A$

Let us use the notation  $\mathbf{A} = [\mathbf{a}_1, \dots, \mathbf{a}_n]$  and let  $[\mathbf{A}]_c$  be the column ordered vectorised form of  $\mathbf{A}$ , namely  $[\mathbf{A}]_c^T = [\mathbf{a}_1^T, \dots, \mathbf{a}_n^T]$ . Then it follows that

$$q_{AZ}(\mathbf{A}, \mathbf{Z}) \propto \exp \left\{ \langle \mathbf{h}_A \rangle_{q_{AZ}}^T [\mathbf{A}]_c - \frac{1}{2} [\mathbf{A}]_c^T \langle \mathbf{Q}_A \rangle_{q_{AZ}} [\mathbf{A}]_c \right\} \times \prod_{ij} p_0(a_{ij}, z_{ij} | \boldsymbol{\theta}), \quad (33)$$

where

$$\begin{aligned} \mathbf{h}_A &= \left[ \mathbf{Q} \sum_t \mathbf{x}_{t+1} \mathbf{x}_t^T - \mathbf{Q} \mathbf{B} \sum_t \mathbf{u}_t \mathbf{x}_t^T \right]_c, \\ \mathbf{Q}_A &= \sum_t \mathbf{x}_t \mathbf{x}_t^T \otimes \mathbf{Q}. \end{aligned}$$

This model is a Gaussian mixture model, thus inference is generally non-tractable because of the exponential growth w.r.t. the dimensionality of  $[\mathbf{A}]_c$ . However, when  $\mathbf{A}$  and  $\mathbf{Q}$  are sparse there is a significant decrease in the effective size of the model ( $[\mathbf{A}]_c$  has a much smaller dimensionality than  $n^2$ ). Moreover, when  $\mathbf{Q}$  is diagonal the distribution  $q_{AZ}(\mathbf{A}, \mathbf{Z})$  factorises over the rows of  $\mathbf{A}$  that is we have  $q_{AZ}(\mathbf{A}, \mathbf{Z}) = \prod_i q_{AZ}(\mathbf{a}_{i,\cdot}, \mathbf{z}_{i,\cdot})$ . In the latter case the number of structural non-zeros in  $\mathbf{a}_{i,\cdot}$  is low, that is  $|I_i|$  typically lower than 10, thus inference can be done exactly—we only have only  $2^{10}$  mixture components of dimension 10. For non-diagonal, but sparse  $\mathbf{Q}$ , we still have a sparse latent Gaussian model with mixture priors and the approximate methods we introduce can be applied.

It is important to note that due to the sparsity of  $\mathbf{A}$ , the rows and columns of both  $\mathbf{h}_A$ ,  $\mathbf{Q}_A$  and  $[\mathbf{A}]_c$  corresponding to structural zeros in  $\mathbf{A}$  can be eliminated. Therefore, the size of the sparse latent Gaussian model—sparsity in  $\mathbf{Q}_A$  follows from the sparsity of  $\mathbf{Q}$ —scales with the number of non-zeros in  $\mathbf{A}$ , that is, around  $n \log n$  instead of  $n^2$ . This inference task can be accommodated by the approximate inference method we present in the following sections.



### 6.3 The model for $q_B$

The model for  $\mathbf{B}$  follows a similar structure and is given by

$$q_B(\mathbf{B}) \propto \exp \left\{ \langle \mathbf{h}_B \rangle_{q_B}^T [\mathbf{B}]_c - \frac{1}{2} [\mathbf{B}]_c^T \langle \mathbf{Q}_B \rangle_{q_B} [\mathbf{B}]_c \right\} \times \prod_{ij} p_0(b_{ij} | \boldsymbol{\theta}) \quad (34)$$

with

$$\mathbf{h}_B = \left[ \mathbf{Q} \sum_t (\mathbf{x}_{t+1} - \mathbf{A} \mathbf{x}_t) \mathbf{u}_t^T \right]_c, \\ \mathbf{Q}_B = \sum_t \mathbf{u}_t \mathbf{u}_t^T \otimes \mathbf{Q}.$$

This model is again a latent Gaussian model where the possible non-Gaussian terms are the priors  $p(b_{ij} | \boldsymbol{\theta})$  and similar simplifications apply as in the previous section.

### 6.4 The model for $q_Q$

This distribution is somewhat more complicated than the rest because it involves a log determinant term, but suitable choices for the structure of  $\mathbf{Q}$  and the prior  $p_0(\mathbf{Q})$  can help to make inference tractable. The distribution  $q_Q$  has the form

$$q_Q(\mathbf{Q}) \propto \exp \left\{ \frac{1}{2} \log \det \mathbf{Q} - \frac{1}{2} \text{tr}(\mathbf{Q}^T \mathbf{H}_Q) \right\} \times p_0(\mathbf{Q} | \boldsymbol{\theta}), \quad (35)$$

where

$$\mathbf{H}_Q = \langle \mathbf{x}_{t+1} \mathbf{x}_{t+1} \rangle_{q_x} - 2 \text{tr} \left\{ \langle \mathbf{A} \rangle_{q_A} \langle \mathbf{x}_t \mathbf{x}_{t+1}^T \rangle_{q_x} \right\} + \text{tr} \left\{ \langle \mathbf{A}^T \mathbf{A} \rangle_{q_A} \langle \mathbf{x}_t \mathbf{x}_t^T \rangle_{q_x} \right\} \\ - 2 \langle \mathbf{B} \rangle_{q_B} \sum_t \mathbf{u}_t (\langle \mathbf{x}_{t+1} \rangle_{q_x} - \langle \mathbf{A} \rangle_{q_A} \langle \mathbf{x}_t \rangle_{q_x})^T + \langle \mathbf{B}^T \mathbf{B} \rangle_{q_B} \sum_t \mathbf{u}_t \mathbf{u}_t^T.$$

In our model we use a diagonal structure with a Gamma prior, therefore inference is analytically tractable.

## 7 Variational inference with expectation constraints

With the exception of  $q_Q$ , all the above models are latent Gaussian models where exact inference can be intractable due to the non-Gaussian prior or likelihood terms. The objective in (26) can be written as

$$F(q_X, q_{AZ}, q_B, q_Q) = - \langle \log p(\mathbf{X}, \mathbf{A}, \mathbf{Z}, \mathbf{Q}, \mathbf{B} | \cdot) \rangle_{q_X, q_{AZ}, q_B, q_Q} - H(q_X) - H(q_{AZ}) - H(q_B) - H(q_Q),$$

where  $H(q)$  denotes the entropy of a distribution  $q$ .

Since we do not have any parametric form for the above densities and we focus on an approximate inference scheme for the marginals, we introduce a sets of approximate marginals for all the involved densities. We then define approximate entropy terms leading to a new objective function to optimise. To ensure consistency, we constrain the approximate marginals to obey expectation constraints up to second order. In the following we motivate and detail our choice for each of the above densities.



## 7.1 Approximate marginals for $q_X$

The distribution  $q_X$  has a chain structured factor graph with additional non-Gaussian terms. For this reason, we define a tree structured family of approximate marginals

$$\mathcal{Q}_x = \{\{q_{t,t+1}^x\}_t, \{q_t^{x,f}\}_t, \{q_{t,j}^x\}_{t,j}, \{q_{t,j}^g\}_{t,j}\}. \quad (36)$$

where we assign the  $q_{t,t+1}^x(\mathbf{x}_t, \mathbf{x}_{t+1})$  to the Gaussian factor  $\Psi_{t,t+1}(\mathbf{x}_t, \mathbf{x}_{t+1})$ , and  $q_{t+1,j}^x(\mathbf{x}_{t+1})$  to the non-Gaussian factor  $\psi_{t+1,j}(\mathbf{x}_{t+1})$ . This family can be viewed as a set of marginals that define a joint tree or chain structured density

$$\tilde{q}_X(\mathbf{X}) \propto \frac{\prod_t q_{t,t+1}^x(\mathbf{x}_t, \mathbf{x}_{t+1})}{\prod_t q_{t+1}^{x,f}(\mathbf{x}_{t+1})} \times \prod_{t,j} \frac{q_{t+1,j}^x(\mathbf{x}_{t+1})}{q_{t+1,j}^{x,g}(\mathbf{x}_{t+1})}.$$

where  $q_t^{x,f}$  and  $q_{t+1,j}^{x,g}$  will denote additional densities over the separator sets in the graphical model and are used to account for the double-counting in the numerator.

Clearly these approximate marginals have to obey consistency constraints, i.e., we  $q_{t-1,t}^x$ ,  $q_{t,t+1}^x$  and  $q_t^{x,f}$  have to be consistent over  $\mathbf{x}_t$  and so must  $q_{t,t+1}^x$ ,  $q_{t+1,t+2}^x$  and  $q_{t+1,j}^{x,g}$  be over  $\mathbf{x}_{t+1}^j$ . Due to non-Gaussianity the marginal consistencies are hard to impose. For this reason, we use weak consistencies such as consistency over certain statistics (expectation constraints). For  $q_{t,t+1}^x$ ,  $q_{t+1,t+2}^x$  and  $q_{t+1,j}^{x,g}$  we postulate expectation constraints  $\mathbf{g}(x_{t+1}^j) = (x_{t+1}^j, -[x_{t+1}^j]^2/2)$ , this helps us to deal with non-Gaussianity, while for  $q_{t-1,t}^x$ ,  $q_{t,t+1}^x$  and  $q_t^{x,f}$  we introduce expectation constraints over a sparse Gaussian Markov random field  $\mathbf{f}(\mathbf{x}_t) = (\{x_t^j\}_i, \{-[x_t^j]^2/2\}_i, \{-x_t^i x_t^j/2\}_{i \sim j})$  where  $i \sim j$  denotes an adjacency relation in a graph  $G(\mathbf{f})$  to be specified later—note that a fully connected  $G(\mathbf{f})$  corresponds to first and second order moments in the state space variable. The choice of  $\mathbf{f}$  (or  $G(\mathbf{f})$ ) depends on the specific model at hand and, as we will see later, our selection criteria will be the tractability of the computations they imply, that is, the sparsity they generate. The weak consistency conditions are thus expressed by the expectation constraints

$$\langle \mathbf{f}(\mathbf{x}_{t+1}) \rangle_{q_{t,t+1}^x} = \langle \mathbf{f}(\mathbf{x}_{t+1}) \rangle_{q_{t+1}^{x,f}} \quad \text{and} \quad \langle \mathbf{f}(\mathbf{x}_{t+1}) \rangle_{q_{t+1,t+2}^x} = \langle \mathbf{f}(\mathbf{x}_{t+1}) \rangle_{q_{t+1}^{x,f}}, \quad (37)$$

as well as

$$\langle \mathbf{g}(\mathbf{x}_{t+1}) \rangle_{q_{t,t+1}^x} = \langle \mathbf{g}(\mathbf{x}_{t+1}) \rangle_{q_{t+1,j}^{x,g}} \quad \text{and} \quad \langle \mathbf{g}(\mathbf{x}_{t+1}) \rangle_{q_{t+1,j}^x} = \langle \mathbf{g}(\mathbf{x}_{t+1}) \rangle_{q_{t+1,j}^{x,g}}. \quad (38)$$

The tree structure of the model implies an entropy approximation

$$-\tilde{H}(\mathcal{Q}_x) = \sum_t \langle \log q_{t,t+1}^x \rangle_{q_{t,t+1}^x} - \sum_t \langle \log q_t^{x,f} \rangle_{q_t^{x,f}} + \sum_{t,j} \langle \log q_{t,j}^x \rangle_{q_{t,j}^x} - \sum_{t,j} \langle \log q_{t,j}^{x,g} \rangle_{q_{t,j}^{x,g}} \quad (39)$$

and Lagrange multiplier terms corresponding to the constraints are defined as

$$\begin{aligned} C(\mathcal{Q}_x, \Lambda_x) = & \sum_t \lambda_{t+1}^\beta \cdot [\langle \mathbf{f}(\mathbf{x}_{t+1}) \rangle_{q_{t,t+1}^x} - \langle \mathbf{f}(\mathbf{x}_{t+1}) \rangle_{q_{t+1}^{x,f}}] + \sum_t \lambda_{t+1}^\alpha \cdot [\langle \mathbf{f}(\mathbf{x}_{t+1}) \rangle_{q_{t,t+1}^x} - \langle \mathbf{f}(\mathbf{x}_{t+1}) \rangle_{q_{t+1,t+2}^x}] \\ & \sum_{t,j} \lambda_{t+1,j}^0 \cdot [\langle \mathbf{g}(\mathbf{x}_{t+1}) \rangle_{q_{t+1,j}^x} - \langle \mathbf{g}(\mathbf{x}_{t+1}) \rangle_{q_{t+1,j}^{x,g}}] + \sum_{t,j} \lambda_{t+1,j}^g \cdot [\langle \mathbf{g}(\mathbf{x}_{t+1}) \rangle_{q_{t+1,j}^x} - \langle \mathbf{g}(\mathbf{x}_{t+1}) \rangle_{q_{t+1,j}^{x,g}}]. \end{aligned} \quad (40)$$

## 7.2 Approximate marginals for $q_{AZ}$

In case of  $q_{AZ}$  we have a latent Gaussian mixture model with the mixture terms  $p_0(a_{ij}, z_{ij}|\boldsymbol{\theta})$  which is again tree structured. For this reason we define a set of approximate marginals

$$\mathcal{Q}_{AZ} = \{q_0^A, \{q_{ij}^{AZ}\}_{ij}, \{q_{ij}^{A,g}\}_{ij}\} \quad (41)$$

where we associate  $q_0^A$  with the exponentiated quadratic form in  $q_A$  and we associate  $q_{ij}^{AZ}(a_{ij}, z_{ij})$  with the prior  $p_0(a_{ij}, z_{ij}|\boldsymbol{\theta})$ . Because of latent Gaussian nature of  $q_A$ , we will require expectation constraints up to second order. That is, we choose  $\mathbf{g}(z) = (z, -z^2/2)$  and we set the constraints  $\langle \mathbf{g}(a_{ij}) \rangle_{q_{ij}^{A,g}} = \langle \mathbf{g}(a_{ij}) \rangle_{q_0^A}$  and  $\langle \mathbf{g}(a_{ij}) \rangle_{q_{ij}^{A,g}} = \langle \mathbf{g}(a_{ij}) \rangle_{q_{ij}^{AZ}}$ . The family  $\mathcal{Q}_A$  defines a set of marginal densities that can be viewed as corresponding to a density written in the form

$$\tilde{q}_{AZ}(\mathbf{A}, \mathbf{Z}) \propto q_0^A(\mathbf{A}) \prod_{ij} \frac{q_{ij}^{AZ}(a_{ij}, z_{ij})}{q_{ij}^{A,g}(a_{ij})}. \quad (42)$$

The corresponding entropy approximation will be defined as

$$-\tilde{H}(\mathcal{Q}_{AZ}) = \langle \log q_0^A \rangle_{q_0^A} + \sum_{ij} \langle \log q_{ij}^{AZ} \rangle_{q_{ij}^{AZ}} - \sum_{ij} \langle \log q_{ij}^{A,g} \rangle_{q_{ij}^{A,g}}, \quad (43)$$

and a set of Lagrangian terms for the expectation constraints can be written as

$$C(\mathcal{Q}_{AZ}, \Lambda_{AZ}) = \sum_{ij} \lambda_{ij}^{A,g} \cdot [\langle \mathbf{g}(a_{ij}) \rangle_{q_{ij}^{A,g}} - \langle \mathbf{g}(a_{ij}) \rangle_{q_{ij}^{AZ}}] + \sum_{ij} \lambda_{ij}^{A,0} \cdot [\langle \mathbf{g}(a_{ij}) \rangle_{q_{ij}^{A,g}} - \langle \mathbf{g}(a_{ij}) \rangle_{q_0^A}]. \quad (44)$$

Note that when  $\mathbf{Q}$  is diagonal  $q_0^A$  factorises. Therefore, the inference problems decouples for each row of  $\mathbf{A}$  leading to sets of independent approximate marginals  $\mathcal{Q}_{AZ}^i$  and corresponding entropy approximations and Lagrangian terms. These decouple as  $\tilde{H}(\mathcal{Q}_{AZ}) = \sum_i \tilde{H}(\mathcal{Q}_{AZ}^i)$

and  $C(\mathcal{Q}_{AZ}, \Lambda_{AZ}) = \sum_i C(\mathcal{Q}_{AZ}^i, \Lambda_{AZ}^i)$ .

## 7.3 Approximate marginals for $q_B$

In case of  $q_B$  we have a similar latent Gaussian model as for  $q_{AZ}$ , except from the discrete mixing variables  $z_{ij}$ , thus we define the family of approximate marginals

$$\mathcal{Q}_B = \{q_0^B, \{q_{ij}^B\}_{ij}, \{q_{ij}^{B,g}\}_{ij}\}. \quad (45)$$

We assign  $q_0^B$  to the exponentiated quadratic form in  $q_B$  and we assign  $q_{ij}^B(b_{ij})$  to the prior  $p_0(b_{ij})$ . The corresponding approximating density can be viewed as

$$\tilde{q}_B(\mathbf{B}) \propto q_0^B(\mathbf{B}) \prod_{ij} \frac{q_{ij}^B(b_{ij})}{q_{ij}^{B,g}(b_{ij})}. \quad (46)$$

We define the expectation constraints in a similar fashion as in case of  $q_{AZ}$ . The approximate entropy term will be

$$-\tilde{H}(\mathcal{Q}_B) = \langle \log q_0^B \rangle_{q_0^B} + \sum_{ij} \langle \log q_{ij}^B \rangle_{q_{ij}^B} - \sum_{ij} \langle \log q_{ij}^{B,g} \rangle_{q_{ij}^{B,g}} \quad (47)$$

and the Langrangian term corresponding to the expectation constraints will be written as

$$C(\mathcal{Q}_B, \Lambda_B) = \sum_{ij} \lambda_{ij}^{B,g} \cdot \left[ \langle \mathbf{g}(b_{ij}) \rangle_{q_{ij}^{B,g}} - \langle \mathbf{g}(b_{ij}) \rangle_{q_{ij}^B} \right] + \sum_{ij} \lambda_{ij}^{B,0} \cdot \left[ \langle \mathbf{g}(b_{ij}) \rangle_{q_{ij}^{B,g}} - \langle \mathbf{g}(b_{ij}) \rangle_{q_0^B} \right]. \quad (48)$$

## 7.4 Approximate marginals for $q_Q$

We do not define any approximation for  $q_Q$ , since we assume that the free form variational update can be done analytically and all the expectation and entropy terms needed are also analytically tractable.

## 7.5 Free energy optimisation and (approximate) message passing

The Lagrangian corresponding to the free energy minimisation expressed in terms of  $\mathcal{Q}_x, \mathcal{Q}_{AZ}, \mathcal{Q}_B$  and  $q_Q$  is written as

$$\begin{aligned} L(\mathcal{Q}_x, \mathcal{Q}_A, \mathcal{Q}_Q, \mathcal{Q}_B, \Lambda_x, \Lambda_A, \Lambda_Q, \Lambda_B) = & -\langle \log p(\mathbf{Y}, \mathbf{X}, \mathbf{A}, \mathbf{Q}, \mathbf{B} | \mathbf{U}) \rangle_{\mathcal{Q}_x, \mathcal{Q}_A, \mathcal{Q}_Q, \mathcal{Q}_B} \\ & - \tilde{H}(\mathcal{Q}_x) - \tilde{H}(\mathcal{Q}_A) - H(q_Q) - \tilde{H}(\mathcal{Q}_B) \\ & + C(\mathcal{Q}_x, \Lambda_x) + C(\mathcal{Q}_A, \Lambda_A) + C(\mathcal{Q}_B, \Lambda_B) + \text{normalisation constraints.} \end{aligned}$$

To differentiate between the free form densities, for example  $q_{AZ}$ , and the corresponding family of marginals, for example  $\mathcal{Q}_A$ , we use a different kind of notation for expectations. The quantities corresponding to  $\mathbf{h}_A$  and  $\mathbf{Q}_A$  will be denoted by  $\langle \mathbf{h}_A \rangle_{\mathcal{Q}_A}$  and  $\langle \mathbf{Q}_A \rangle_{\mathcal{Q}_A}$  and the same rule applies for  $q_B$  and  $\mathcal{Q}_B$ . For  $q_x$  and  $\mathcal{Q}_x$  we use the shortcut notation  $\langle \log \Psi_{t,t+1}(\mathbf{x}_t, \mathbf{x}_{t+1}) \rangle_{\mathcal{Q}_x}$ , but the same usage applies.

From the stationary conditions of  $L$  w.r.t the members of the families  $\mathcal{Q}_x, \mathcal{Q}_{AZ}$  and  $\mathcal{Q}_B$  we can derive the form of the approximating densities. The stationarity conditions corresponding to the expectation constraints will be used to define a message passing algorithm. We turn the stationary conditions of the Lagrangian into a fixed point iteration over the Lagrange multipliers and try to find stable fixed point. The iteration typically converges in practice and results in good quality approximations as shown in the main body of the paper.

(1) For the members of the family  $\mathcal{Q}_x$  we have

$$q_{t,t+1}^x(\mathbf{x}_t, \mathbf{x}_{t+1}) \propto \exp \left\{ \langle \log \Psi_{t,t+1}(\mathbf{x}_t, \mathbf{x}_{t+1}) \rangle_{\mathcal{Q}_x} \right. \quad (49)$$

$$\left. + \lambda_t^\alpha \cdot \mathbf{f}(\mathbf{x}_t) + \lambda_{t+1}^\beta \cdot \mathbf{f}(\mathbf{x}_{t+1}) + \sum_j \lambda_{t+1,j}^0 \cdot \mathbf{g}(\mathbf{x}_{t+1}) \right\}, \quad (50)$$

$$q_{t+1,j}^x(x_{t+1}^j) \propto \psi_{t+1,j}(x_{t+1}^j) \times \exp \{ \lambda_{t+1,j}^g \cdot \mathbf{g}(x_{t+1}^j) \}, \quad (51)$$

$$q_{t+1,j}^{x,g}(x_{t+1}^j) \propto \exp \{ (\lambda_{t+1,j}^0 + \lambda_{t+1,j}^g) \cdot \mathbf{g}(x_{t+1}^j) \}, \quad (52)$$

$$q_{t+1}^{x,f}(\mathbf{x}_{t+1}) \propto \exp \{ (\lambda_{t+1}^\alpha + \lambda_{t+1}^f) \cdot \mathbf{f}(\mathbf{x}_{t+1}) \}, \quad (53)$$

We note that both  $q_{t+1,j}^{x,g}(x_{t+1}^j)$  and  $q_{t+1}^{x,f}(\mathbf{x}_{t+1})$  are Gaussian densities, therefore, by defining the moment matching KL projection

$$\text{Project}[p(\mathbf{z}); \mathbf{f}] = \underset{\boldsymbol{\theta}}{\text{argmin}} \mathbb{D}[p(\mathbf{z}) || \exp(\boldsymbol{\theta} \cdot \mathbf{f}(\mathbf{z}) - \log Z(\boldsymbol{\theta}))],$$

we can turn the expectation constraints into the fixed point updates

$$[\lambda_{t+1,j}^g]^{new} = \text{Project}(q_{t,t+1}^x[\mathbf{x}_{t+1}]; \mathbf{g}) - \lambda_{t+1,j}^0, \quad (54)$$

$$[\lambda_{t+1,j}^0]^{new} = \text{Project}(q_{t+1,j}^x[\mathbf{x}_{t+1}]; \mathbf{g}) - \lambda_{t+1,j}^g, \quad (55)$$

$$[\lambda_{t+1}^\alpha]^{new} = \text{Project}(q_{t,t+1}^x[\mathbf{x}_{t+1}]; \mathbf{f}) - \lambda_{t+1}^\beta, \quad (56)$$

$$[\beta_{t+1}^\alpha]^{new} = \text{Project}(q_{t+1,t+2}^x[\mathbf{x}_{t+1}]; \mathbf{f}) - \lambda_{t+1}^\alpha. \quad (57)$$

(2) For the members of the family  $\mathcal{Q}_{AZ}$  we have

$$q_0^A([\mathbf{A}]_c) \propto \exp \left\{ [\mathbf{A}]_c^T \langle \mathbf{h}_A \rangle_{\mathcal{Q}_A} - \frac{1}{2} [\mathbf{A}]_c^T \langle \mathbf{Q}_A \rangle_{\mathcal{Q}_A} [\mathbf{A}]_c + \sum_{ij} \lambda_{ij}^{A,0} \cdot \mathbf{g}(a_{ij}) \right\}, \quad (58)$$

$$q_{ij}^{AZ}(a_{ij}, z_{ij}) \propto p_0(a_{ij}, z_{ij} | \boldsymbol{\theta}) \times \exp \left\{ \lambda_{ij}^{A,g} \cdot \mathbf{g}(a_{ij}) \right\}, \quad (59)$$

$$q_{ij}^{A,g}(a_{ij}) \propto \exp \left\{ (\lambda_{ij}^{A,0} + \lambda_{ij}^{A,g}) \cdot \mathbf{g}(a_{ij}) \right\}, \quad (60)$$

and the corresponding expectation constraints lead to the equations

$$[\lambda_{ij}^{A,0}]^{new} = \text{Project}[q_{ij}^{AZ}(a_{ij}); \mathbf{g}] - \lambda_{ij}^{A,g}, \quad (61)$$

$$[\lambda_{ij}^{A,g}]^{new} = \text{Project}[q_0^A(a_{ij}); \mathbf{g}] - \lambda_{ij}^{A,0}. \quad (62)$$

(3) For the members of the family  $\mathcal{Q}_B$  we have

$$q_0^B([\mathbf{B}]_c) \propto \exp \left\{ [\mathbf{B}]_c^T \langle \mathbf{h}_B \rangle_{\mathcal{Q}_B} - \frac{1}{2} [\mathbf{B}]_c^T \langle \mathbf{Q}_B \rangle_{\mathcal{Q}_B} [\mathbf{B}]_c + \sum_{ij} \lambda_{ij}^{B,0} \cdot \mathbf{g}(b_{ij}) \right\}, \quad (63)$$

$$q_{ij}^B(b_{ij}) \propto p_0(b_{ij} | \boldsymbol{\theta}) \times \exp \left\{ \lambda_{ij}^{B,g} \cdot \mathbf{g}(b_{ij}) \right\}, \quad (64)$$

$$q_{ij}^{B,g}(b_{ij}) \propto \exp \left\{ (\lambda_{ij}^{B,0} + \lambda_{ij}^{B,g}) \cdot \mathbf{g}(b_{ij}) \right\}, \quad (65)$$

and the corresponding expectation constraints lead to the update equations

$$[\lambda_{ij}^{B,0}]^{new} = \text{Project}[q_{ij}^B(b_{ij}); \mathbf{g}] - \lambda_{ij}^{B,g}, \quad (66)$$

$$[\lambda_{ij}^{B,g}]^{new} = \text{Project}[q_0^B(b_{ij}); \mathbf{g}] - \lambda_{ij}^{B,0}. \quad (67)$$

We run the fixed point updates according to the variational Bayes approach, that is, for each set of marginals  $\mathcal{Q}_X$ ,  $\mathcal{Q}_{AZ}$ ,  $\mathcal{Q}_B$  we run the corresponding updates until convergence and then we proceed to the next family. The details of the projection operations and message scheduling are presented in the main body of the paper.

Note that when the inference can be done exactly as it is the case for  $q_{AZ}^i$  or Gaussian  $p(b_{ij})$ , then the projection operations are simply replaced by the corresponding free form variational update as presented in Section 6. This corresponds to replacing the approximate entropies with the exact ones and omitting the introduction of the families of approximate marginals and the corresponding expectation constraints.

## 7.6 Sparse approximations with known structure for $\mathbf{A}$ and $\mathbf{Q}$

In this section we discuss the sparsity issues that are essential for the scalability of the algorithm we propose. The basic assumption we start from is that both  $\mathbf{A}$  and  $\mathbf{Q}$  are sparse. We assume that  $\mathbf{B}$  is a full matrix, although if we want to assume some structural sparsity, the issue can be addressed in the same way as for  $\mathbf{A}$ .

A crucial observation is that in all projections steps we perform, we act on a sparse precision matrix and we compute all covariance values corresponding to the non-zero positions in this precision matrix. We argue that these covariance values are sufficient to keep the algorithm running, that is, there is no need to compute extra covariances and that the covariances we compute always lead to positive semi-definite precision matrices. Given our observation about the computation of the covariances, the first argument is quite intuitive: wherever there is a term with quadratic interaction between two variables of the same type be it  $\mathbf{X}$ ,  $\mathbf{A}$ ,  $\mathbf{B}$  the moments of the other variables interacting with them are computed by their corresponding inference scheme and thus this property is conserved. The second argument related to positive (semi)-definiteness requires a closer look.

First we explore the connection between  $\mathbf{X}$  and  $\mathbf{A}$ . We have  $\langle \mathbf{Q}_{t,t+1}^x \rangle_{\mathcal{Q}_x} = \langle \mathbf{Q}_{t,t+1}^x \rangle_{q_0^A q_Q}$ . Since  $(\mathbf{x}_{t+1} - \mathbf{A}\mathbf{x}_t)^T \mathbf{Q} (\mathbf{x}_{t+1} - \mathbf{A}\mathbf{x}_t) \geq 0$  for any  $\mathbf{x}_t, \mathbf{x}_{t+1}, \mathbf{A}$  and positive semi-definite  $\mathbf{Q}$ , it follows that  $\langle (\mathbf{x}_{t+1} - \mathbf{A}\mathbf{x}_t)^T \langle \mathbf{Q} \rangle_{q_Q} (\mathbf{x}_{t+1} - \mathbf{A}\mathbf{x}_t) \rangle_{q_0^A} \geq 0$  for any positive semi-definite  $\langle \mathbf{Q} \rangle_{q_Q}$  thus  $\langle \mathbf{Q}_{t,t+1}^x \rangle_{\mathcal{Q}_x}$  is positive semi-definite for all semi-definite  $\langle \mathbf{Q} \rangle_{q_Q}$ . The argument for  $\langle \mathbf{Q}_A \rangle_{\mathcal{Q}_A}$  is as follows: first we construct the matrix  $\sum_t \langle \mathbf{x}_t \mathbf{x}_t^T \rangle_{\mathcal{Q}_x} \otimes \langle \mathbf{Q} \rangle_{q_Q} = \sum_t \langle \mathbf{x}_t \mathbf{x}_t^T \rangle_{q_{t,t+1}^x} \otimes \langle \mathbf{Q} \rangle_{q_Q}$  which, since it is a Kronecker product of positive semi-definite matrices, it is also positive semi-definite. Now, by eliminating the rows and columns corresponding to the a-priori set structural zeros in  $[\mathbf{A}]_c$  we arrive to a principal minor that also has to be positive semi-definite. The  $(i, j)$  block of  $\langle \mathbf{Q}_A \rangle_{\mathcal{Q}_A}$  is  $\langle x_t^i x_t^j \rangle [\langle \mathbf{Q} \rangle_{q_Q}]_{I_i, I_j}$  where  $I_i$  and  $I_j$  are the supports of  $\mathbf{a}_i$  and  $\mathbf{a}_j$  respectively. Since the elements of  $\mathbf{A}^T \mathbf{Q} \mathbf{A}$  are  $\mathbf{a}_{I_i, i}^T \mathbf{Q}_{I_i, I_j} \mathbf{a}_{I_j, j}$ , it follows that  $\langle x_t^i x_t^j \rangle$  is always computed when needed, that is, when  $I_i \cap I_j \neq \emptyset$ . This shows that the sparsity structures can be exploited and that the resulting inference keeps the matrices positive semi-definite.

## 7.7 Notes about the convergence

We have no convergence guarantees for the method we introduce, and neither are there convergence guarantees in the literature for the particular parts  $q_X, q_B$  and  $q_{AZ}$ . It has been shown that when the non-Gaussian terms  $\psi_{t,j}(x_t^j)$  are log-concave (the  $q_X$  is unimodal), then the block version of the model for  $q_X$  does not diverge (Seeger, 2008). This property can be adapted to the distributed/dynamic inference approach we present in the paper. Similar arguments apply for the model  $q_B$  when  $p(b_{ij})$  are log-concave. The approximate inference method for  $q_{AZ}$  is less robust, however, it has been applied in several models such as robust regression (Kuss et al., 2005) and variables selection (e.g. Hernández-Lobato et al., 2013). It is known to behave generally well by using some additional techniques to stabilise the fixed point update in (61) and (62). One common technique is called damping (e.g. Heskes, 2004),

where we choose  $\epsilon \in [0, 1]$  and use the update

$$[\lambda_{ij}^{A,0}]^{new} = (1 - \epsilon)[\lambda_{ij}^{A,0}] + \epsilon(\text{Project}[q_{ij}^{AZ}(a_{ij}); \mathbf{g}] - \lambda_{ij}^{A,g}),$$

while the other one arises from a modified entropy approximation which results in the update

$$\begin{aligned} [\lambda_{ij}^{A,0}]^{new} &= \frac{1}{\eta}(\text{Project}[q_{ij}^{AZ}(a_{ij}); \mathbf{g}] - \lambda_{ij}^{A,g}), \\ [\lambda_{ij}^{A,g}]^{new} &= \text{Project}[q_0^A(a_{ij}); \mathbf{g}] - \eta \lambda_{ij}^{A,0}, \end{aligned}$$

where again we have  $\eta \in [0, 1]$ . The latter technique is related to the, so called, fractional belief or expectation propagation and convexified entropy approximations (Wiegerinck and Heskes, 2003; Wainwright et al., 2003; Minka, 2004; Heskes, 2006).

The only convergence issue we had was related to the convergence of *diag* for  $q_X$ . In some models with strong correlations in  $\tilde{q}_X(\mathbf{x}_t, \mathbf{x}_{t+1})$  we applied a damping of  $\epsilon = 0.9$  for the temporal messages  $\alpha_t$  and  $\beta_t$ . To infer  $\mathbf{A}$  (Section 4.2 of the paper), we applied both the exact inference and the message passing presented above for a diagonal  $\mathbf{Q}$  and the result were very similar.

## References

- C. Andrieu, A. Doucet, and R. Holenstein. Particle Markov chain Monte Carlo methods. *Journal of the Royal Statistical Society (Series B)*, 72(3), 2010.
- P. Baudains, S. D. Johnson, and A. M. Braithwaite. Geographic patterns of diffusion in the 2011 London riots. *Applied Geography*, 45:211–219, 2013.
- A. Brix and Møller. Space-time multi type log gaussian cox processes with a view to modelling weeds. *Scandinavian Journal of Statistics*, 28(3):471–488, 2001.
- D. Bueche, N. Sukumar, and B. Moran. Dispersive properties of the natural element method. *Computational Mechanics*, 25(2):207–219, 2000.
- B. Cseke and T. Heskes. Approximate marginals in latent Gaussian models. *Journal of Machine Learning Research*, 12:417–454, 2011.
- J. Dahl, L. Vandenberghe, and V. Roychowdhury. Covariance selection for non-chordal graphs via chordal embedding. *Optimization Methods Software*, 23(4):501–520, 2008.
- T. A. Davis. *Direct Methods for Sparse Linear Systems (Fundamentals of Algorithms 2)*. Society for Industrial and Applied Mathematics, Philadelphia, PA, USA, 2006.
- P. Diggle, B. Rowlingson, and T. Su. Point process methodology for on-line spatio-temporal disease surveillance. *Environmetrics*, 16(5):423–434, 2005.
- M. Gerven, B. Cseke, R. Oostenveld, and T. Heskes. Bayesian source localization with the multivariate Laplace prior. In *Advances in Neural Information Processing Systems 22*, pages 1901–1909, 2009.

- M. Gerven, A. Bahramisharif, J. Farquhar, and T. Heskes. Donders machine learning toolbox, 2012. URL <https://github.com/distrep/DMLT>.
- M. Girolami and B. Calderhead. Riemann manifold Langevin and Hamiltonian Monte Carlo methods. *Journal of the Royal Statistical Society (Series B)*, 73(2):123–214, 2011.
- J. Hartikainen, J. Riihimäki, and S. Särkkä. Sparse spatio-temporal Gaussian processes with general likelihoods. In *Proceedings of the 21th International Conference on Artificial Neural Networks*, pages 193–200, 2011.
- D. Hernández-Lobato, J. M. Hernández-Lobato, and P. Dupont. Generalized spike-and-slab priors for bayesian group feature selection using expectation propagation. *Journal of Machine Learning Research*, 14(1):1891–1945, 2013.
- T. Heskes. On the uniqueness of loopy belief propagation fixed points. *Neural Computation*, 16:2379–2413, 2004.
- T. Heskes. Convexity arguments for efficient minimization of the Bethe and Kikuchi free energies. *Journal of Artificial Intelligence Research*, 26(1), June 2006.
- T. Heskes and O. Zoeter. Expectation propagation for approximate inference in dynamic Bayesian networks. In *Proceedings of the 18th Conference in Uncertainty in Artificial Intelligence*, pages 216–223, 2002.
- T. Heskes, M. Oppier, W. Wiegerinck, O. Winther, and O. Zoeter. Approximate inference techniques with expectation constraints. *Journal of Statistical Mechanics: Theory and Experiment*, 2005.
- M. B. Hooten and C. K. Wikle. A hierarchical Bayesian non-linear spatio-temporal model for the spread of invasive species with application to the Eurasian Collared-Dove. *Environmental and Ecological Statistics*, 15(1):59–70, 2008.
- F. R. Kschischang, B. J. Frey, and H. A. Loeliger. Factor graphs and the sum-product algorithm. *IEEE Transactions on Information Theory*, 47(2), February 2001.
- M. Kuss and C. E. Rasmussen. Assessing approximate inference for binary Gaussian process classification. *Journal of Machine Learning Research*, 6:1679–1704, 2005.
- M. Kuss, T. Pfingsten, L. Csato, and C. E. Rasmussen. Approximate inference for robust Gaussian process regression. Technical Report 136, Max Planck Institute for Biological Cybernetics, 2005.
- S. L. Lauritzen. *Graphical Models*. Oxford Statistical Science Series. Oxford University Press, New York, USA, 1996.
- F. Lindgren, H. Rue, and J. Lindström. An explicit link between Gaussian fields and Gaussian Markov random fields: the stochastic partial differential equation approach. *Journal of the Royal Statistical Society (Series B)*, 73(4):423–498, 2011.



- T. P. Minka. *A family of algorithms for approximate Bayesian inference*. PhD thesis, MIT, 2001.
- T. P. Minka. Power EP. Technical report, Microsoft Research Ltd., Cambridge, UK, MSR-TR-2004-149, October 2004.
- J. Møller, A. R. Syversveen, and R. P. Waagepetersen. Log-Gaussian Cox processes. *Scandinavian Journal of Statistics*, 25(3):451–482, 1998.
- K. P. Murphy and Y. Weiss. The factored frontier algorithm for approximate inference in dbns. In *Proceedings of the 17th Conference in Uncertainty in Artificial Intelligence*, pages 378–385, 2001.
- M. Opper and O. Winther. Gaussian processes for classification: Mean-field algorithms. *Neural Computation*, 12(11):2655–2684, 2000.
- M. Opper and O. Winther. Expectation consistent approximate inference. *Journal of Machine Learning Research*, 6:2177–2204, 2005.
- P.O. Persson and G. Strang. A simple mesh generator in MATLAB. *SIAM review*, pages 329–345, 2004.
- C. K. I. Rasmussen, C. E. and Williams. *Gaussian Processes for Machine Learning (Adaptive Computation and Machine Learning)*. The MIT Press, 2005.
- H. Rue, S. Martino, and N. Chopin. Approximate Bayesian inference for latent Gaussian models by using integrated nested Laplace approximations. *Journal of The Royal Statistical Society (Series B)*, 71(2):319–392, 2009.
- S. Schutte and N. B. Weidmann. Diffusion patterns of violence in civil wars. *Political Geography*, 30:143–152, 2011.
- M. W. Seeger. Bayesian inference and optimal design for the sparse linear model. *Journal of Machine Learning Research*, 9:759–813, 2008. ISSN 1533-7928.
- D. Simpson, J. Illian, F. Lindgren, S. Sørbye, and H. Rue. Going off grid: Computationally efficient inference for log-Gaussian Cox processes. *arXiv:1111.0641*, 2011.
- D. Simpson, F. Lindgren, and H. Rue. In order to make spatial statistics computationally feasible, we need to forget about the covariance function. *Environmetrics*, 23(1):65–74, 2012.
- D. Simpson, I. W. Turner, C. M. Strickland, and A. N. Pettitt. Scalable iterative methods for sampling from massive gaussian random vectors. *arXiv:1312.1476*, 2013.
- K. Takahashi, J. Fagan, and M.-S. Chin. Formation of a sparse impedance matrix and its application to short circuit study. In *Proceedings of the 8th PICA Conference*, 1973.

- M. Wainwright, T. Jaakkola, and A. Willsky. Tree-reweighted belief propagation algorithms and approximate ML estimation via pseudo-moment matching. In *Proceedings of the Ninth International Workshop on Artificial Intelligence and Statistics*, 2003.
- W. Wiegerinck and T. Heskes. Fractional belief propagation. In S. Becker, S. Thrun, and K. Obermayer, editors, *Advances in Neural Information Processing Systems 15*, pages 438–445, Cambridge, MA, 2003. The MIT Press.
- C. K. Wikle. A kernel-based spectral model for non-Gaussian spatio-temporal processes. *Statistical Modelling*, 2(1):299–314, 2002.
- C. K. Wikle, R. F. Milliff, D. Nychka, and L. M. Berliner. Spatiotemporal hierarchical bayesian modeling tropical ocean surface winds. *Journal of the American Statistical Association*, 96(454):382–397, 2001.
- T. Wist and H. Rue. Specifying a Gaussian markov random field by a sparse Cholesky triangle. *Communications in Statistics: Simulation and Computation*, 35(1):161–176, 2006.
- J. S. Yedidia, W. T. Freeman, and Y. Weiss. Generalized belief propagation. In *Advances in Neural Information Processing Systems 12*, pages 689–695. The MIT Press, 2000.
- A. Ypma and T. Heskes. Novel approximations for inference in nonlinear dynamical systems using expectation propagation. *Neurocomputing*, 69(1):85–99, 2005.
- A. Zammit-Mangion, G. Dewar, M., V. Kadirkamanathan, , and G. Sanguinetti. Point process modelling of the Afghan war diary. *Proceeding of the National Academy of Sciences*, 109(31):12414–12419, 2012a.
- A. Zammit-Mangion, G. Sanguinetti, and V. Kadirkamanathan. Variational estimation in spatiotemporal systems from continuous and point-process observations. *IEEE Transactions on Signal Processing*, 60(7):3449–3459, 2012b.
- O. Zoeter and T. Heskes. Gaussian quadrature based expectation propagation. In Z. Ghahramani and R. Cowell, editors, *Proceedings of the Tenth International Workshop on Artificial Intelligence and Statistics*, pages 445–452, 2005.